

## Influence of transport uncertainty on annual mean and seasonal inversions of atmospheric CO<sub>2</sub> data

Philippe Peylin

Laboratoire de Biogéochimie isotopique, Centre National de la Recherche Scientifique, Université Pierre et Marie Curie, Paris, France

David Baker and Jorge Sarmiento

Atmospheric and Oceanic Sciences Program, Princeton University, Princeton, New Jersey, USA

Philippe Ciais and Philippe Bousquet

Laboratoire des Sciences du Climat et de l'Environnement, Commissariat à l'Energie Atomique, L'orme des merisiers, Gif sur Yvette, France

Received 21 May 2001; revised 19 December 2001; accepted 23 January 2002; published 8 October 2002.

[1] Inversion methods are often used to estimate surface CO<sub>2</sub> fluxes from atmospheric CO<sub>2</sub> concentration measurements, given an atmospheric transport model to relate the two. The published estimates disagree strongly on the location of the main sources and sinks, however. Are these differences due to the different time spans considered, or are they artifacts of the method and data used? Here we assess the uncertainty in such estimates due to the choice of time discretization of the measurements and fluxes, the spatial resolution of the fluxes, and the transport model. A suite of 27 Bayesian least squares inversions has been run, given by varying the number of flux regions solved for (7, 12, and 17), the time discretization (annual/annual, annual/monthly, and monthly/monthly for the fluxes/data), and the transport model (TM2, TM3, and GCTM), while holding all other inversion details constant. The estimated fluxes from this ensemble of inversions for the land + ocean sum are stable over large zonal bands, but the spread in the results increases when considering the longitudinal flux distribution inside these bands. On average for 1990–1994 the inversions place a large CO<sub>2</sub> uptake north of 30°N ( $3.2 \pm 0.3$  GtC yr<sup>-1</sup>), mostly over the land regions, with more in Eurasia than North America. The ocean fluxes are generally smaller than given by *Takahashi et al.* [1999], especially south of 15°S and in the global total, where they are less than half as large. A small uptake is found for the tropical land regions, suggesting that growth more than compensates for deforestation there. The results for the different transport models are consistent with their known mixing properties; the longitudinal pattern of their land biosphere rectifier, in particular, strongly influences the regional partitioning of the flux in the north. While differences between the transport models contribute significantly to the spread of the results, an equivalent or even larger spread is due to the time discretization method used: Solving for annual mean fluxes with monthly mean measurements tended to give spurious land/ocean flux partition in the north. We suggest then that this time discretization method be avoided. Overall, the uncertainty quoted for the estimated fluxes should include not only the random error calculated by the inversion equations but also all the systematic errors in the problem, such as those addressed in this study.

**INDEX TERMS:** 0322 Atmospheric Composition and Structure: Constituent sources and sinks; 1615 Global Change: Biogeochemical processes (4805); 1610 Global Change: Atmosphere (0315, 0325); **KEYWORDS:** atmospheric inversions, carbon cycle, tracer transport model

**Citation:** Peylin, P., D. Baker, J. Sarmiento, P. Ciais, and P. Bousquet, Influence of transport uncertainty on annual mean and seasonal inversions of atmospheric CO<sub>2</sub> data, *J. Geophys. Res.*, 107(D19), 4385, doi:10.1029/2001JD000857, 2002.

### 1. Introduction

[2] Understanding the global carbon cycle is a key priority in current environmental research because of the central

role it plays in regulating global warming. Our best estimates of the amount of anthropogenic CO<sub>2</sub> being taken up by the oceans or remaining in the atmosphere are not large enough to account for all of the emissions [*Tans et al.*, 1990]. The land biosphere is presumably taking up the remainder, but the partitioning of this so-called “missing sink” between the different ecosystems is rather uncertain.

**Table 1.** Recent Inverse Results for the Net CO<sub>2</sub> Uptake by the Land Biosphere

Reference	Sites	Period	Total	Europe	Siberia	N. Amer.	Trop.
<i>Bousquet et al.</i> [1999a, 1999b]	77	85–95	$-1.3 \pm 1.6$	$-0.3 \pm 0.8$	$-1.5 \pm 0.7$	$-0.3 \pm 0.5$	$0.8 \pm 1.0$
<i>Peylin et al.</i> [1999]	53	90–95	$-1.2 \pm 2.8$	$-0.6 \pm 1.5$	$-0.8 \pm 1.2$	$-1.0 \pm 1.2$	$1.2 \pm 1.2$
<i>Rayner et al.</i> [1999]	13	80–95	$-0.7 \pm ?$	$-0.2 \pm ?$	$-0.1 \pm ?$	$-0.5 \pm ?$	$0.1 \pm ?$
<i>Kaminski et al.</i> [1999]	25	81–87 <sup>a</sup>	$-1.0 \pm 0.5$	$-0.1 \pm 0.2$	$-0.6 \pm 0.3$	$-0.2 \pm 0.3$	$-0.1 \pm ?$
<i>Fan et al.</i> [1998]	63	88–92 <sup>a</sup>	$-1.6 \pm 1.7$	$-0.1 \pm 0.7$		$-1.7 \pm 0.5$	$0.2 \pm 0.9$

<sup>a</sup>El Niño removed.

Given large differences in CO<sub>2</sub> residence time between different ecosystems (much longer for boreal forests than tropical forests) [*Kicklighter et al.*, 1999], predicting future CO<sub>2</sub> levels requires a better characterization of the spatial distribution of the carbon sources and sinks. So far, a large part of our knowledge comes from the use of measured atmospheric CO<sub>2</sub> concentrations at different locations. Spatial and temporal concentration differences relate to the surface sources and sinks through the atmospheric mixing. Retrieving the surface fluxes from atmospheric measurements is a typical inverse problem [*Enting*, 1999].

[3] Recent inverse studies have given rather conflicting results for the mean carbon balance of the past 2 decades. Table 1 details these estimates for the land biosphere. Except for broad general feature like global totals for large latitudinal bands, there is no general agreement when considering large continental areas, even for inversions that cover similar time periods (e.g., *Bousquet et al.* [1999a] found a sink of 1.8 GtC yr<sup>-1</sup> for Eurasia plus Siberia, while *Rayner et al.* [1999] and *Fan et al.* [1998] obtained only a 0.3 and a 0.1 GtC yr<sup>-1</sup> sink there). Why are the estimates so different? Clearly, we must try to understand the capabilities and limits of current inverse approaches. Whether the current inversions are able to estimate carbon fluxes at the continental and ocean basin scale or not is a crucial issue.

[4] In this study, we have investigated the main sources of differences between commonly used inverse approaches (like the studies in Table 1) and have tried to identify the most sensitive components. How do transport uncertainties affect the estimated fluxes? What is the influence of the temporal resolution (data and fluxes) and the spatial resolution (fluxes) in the inverse procedure? How should we include independent information on the global ocean uptake, obtained from other trace gases, in the inversion? To achieve these goals, we conducted a series of inversions, based on the Bayesian synthesis approach [*Enting et al.*, 1995], in which we successively changed particular components in the setup of the inverse procedure (transport model, time discretization method, and spatial resolution).

[5] The remainder of the paper is divided into three parts. We first describe the different components of the ensemble of inversions that was conducted. We then present the estimated fluxes, starting from the most robust features to the more highly uncertain ones. Finally, we discuss the contribution of all investigated parameters to the overall spread of the results.

## 2. Methodology

[6] One of the major goals of this study is to investigate which differences in method between several recently published inversion approaches contribute significantly to the

differences in their estimated fluxes (Table 1). To investigate this, we performed a suite of inversions in which we successively modified one parameter or component of the inversion, while keeping the others fixed. After a brief presentation of the inverse technique we review in this section the different characteristics of the inversions, focusing especially on the parameters that we varied. The list of parameters or inversion settings that we explored includes the atmospheric transport model, the spatial discretization of the fluxes solved for (here the number of source regions), the temporal resolution of the fluxes (annual or seasonal), and the influence of constraints on the global ocean uptake.

### 2.1. Bayesian Synthesis Inversion

[7] We use the “Bayesian synthesis technique” [*Enting et al.*, 1995; *Rayner et al.*, 1999; *Bousquet et al.*, 1999a; *Baker*, 1999; *Peylin et al.*, 1999; *Kaminski et al.*, 1999] to perform our inversions. This technique seeks the linear combination of fluxes that yields modeled concentration fields that best match the observational data. It estimates the errors of the inferred fluxes and allows one to include a priori estimates of the flux magnitudes. Seasonally varying fluxes are subdivided into individual sources, each corresponding to a region or to a specific type of emission; these sources are run through an atmospheric transport model to compute their effect on atmospheric CO<sub>2</sub> concentrations at the monitoring stations. The annual or monthly magnitudes of all sources ( $x$ ) are then optimized by minimizing the cost function,

$$J(x) = \frac{1}{2} \left[ (Hx - y^o)^T (R^o)^{-1} (Hx - y^o) + (x - x^b)^T (P^b)^{-1} (x - x^b) \right], \quad (1)$$

where  $Hx$  and  $y^o$  are the vectors of the modeled and observed CO<sub>2</sub> concentrations and  $x^b$  is a vector of the a priori fluxes.  $R^o$  and  $P^b$  denote the covariance matrices for the errors assumed in of  $y^o$  and  $x^b$ , respectively (they are taken to be diagonal here). The second term in equation (1) penalizes deviations of the estimate from the a priori flux values: This term (which characterizes the Bayesian approach) regularizes the problem; that is, it ensures the existence of a unique, well-defined minimum of  $J(x)$ . An overview of this technique can be found in *Enting et al.* [1993].

### 2.2. Temporal Discretization of the Data and Fluxes

[8] In the synthesis inversion technique the degree of temporal discretization of the concentration  $y^o$  and the sources  $x$  is at the discretion of the modeler: The modeler might specify the time-dependence of the fluxes completely

or, at the other extreme, might choose to solve for the fluxes on a daily (or even shorter) basis. Among recent inverse studies, two discretizations have been used most frequently for  $x$  and  $y^o$ : annual and monthly. Figure 1 summarizes four different inversion setups that can be derived from these resolutions and that have been examined in this study. The terminology used was introduced by *Peylin et al.* [1999].

1. The first inversion setup is the annual adjustment with annual data, denoted T1a (time-independent adjustment). In such an inversion, only the annual magnitude of each source is optimized. The temporal pattern of the fluxes (the seasonality) is specified a priori, and a single multiple of this pattern is solved for. The modeled concentrations are averaged into one annual value that is then compared with the observed annual mean concentration at each site. The studies of *Fan et al.* [1998] and *Gloor et al.* [2000] follow this approach.

2. The second setup is the annual adjustment with monthly data, denoted T1m. In such an inversion, as in the T1a case, the fluxes for each region are solved for as a multiple of a prespecified temporal pattern. However, in this case the modeled concentrations are optimized against 12 monthly data averages at each station, instead of a single annual value. The strong seasonality of the atmospheric CO<sub>2</sub> concentration in the Northern Hemisphere thus becomes an additional constraint to the inverse problem, compared with the T1a case. It is important to note that the inferred fluxes in this case should differ from those of the T1a case because of the use of the least squares minimization (i.e., a quadratic  $J(x)$ ). If we were minimizing simple differences (absolute values) between the modeled and observed concentrations, the results would be identical between the T1a and T1m methods. The T1a case averages both data and response functions of the T1m case so that the inversion behavior could be quite different in the least squares framework. Note that in the T1m method, there are 12 times more constraints than in the T1a method. The studies of *Hein et al.* [1997], *Bousquet et al.* [1999a, 1999b], *Taguchi* [1999], and *Ciais et al.* [1998] follow this approach, while *Enting et al.* [1995] used a similar method, solving for several frequencies rather than 12 monthly fluxes.

3. The third setup is the monthly adjustment with monthly data, denoted TDm (TD for time-dependent adjustment). Note that this terminology has also been used to describe interannual variability, whereas we only consider intra-annual variability here. In such an inversion, monthly source magnitudes are solved for, as opposed to in the two preceding TI cases, for which the relative temporal patterns were specified. Because 12 times more flux parameters are solved for, this inversion gives modeled concentrations that fit the observed ones better than in the T1m method. The studies of *Peylin et al.* [1999], *Rayner et al.* [1999], *Baker* [1999], *Kaminski et al.* [1999], *Bousquet et al.* [2000], and *Baker* [2001] follow this approach.

4. The fourth setup is the monthly adjustment with annual data, denoted TDa. In such an inversion the number of sources to be optimized tends to be larger than the number of observational constraints. Given the 46 observational sites used in this study for a case in which fluxes from 7 regions are solved for, the TDa inversion would have only 46 observations to constrain 84 sources (7 regions  $\times$  12

<b>Data</b> <b>Sources</b>	<b>Annual [CO<sub>2</sub>]</b> <b>(a)</b>	<b>Monthly [CO<sub>2</sub>]</b> <b>(m)</b>
<b>Annual adjustment</b> <b>(TI)</b>	46 data $n$ fluxes	46 * 12 data $n$ fluxes
<b>Monthly adjustment</b> <b>(TD)</b>	<del>46 data <math>n</math> * 12 fluxes</del>	46 * 12 data $n$ * 12 fluxes

**Figure 1.** Temporal discretization for the data and sources used for these inversions (either annual or monthly) and the corresponding numbers of atmospheric constraints and sources to solve for. The labels T1a, T1m, and TDm will refer to annual adjustment with annual data, annual adjustment with monthly data, and monthly adjustment with monthly data, respectively. Note that the TDa case is not generally used since it is largely underconstrained.

months). If an a priori constraint were not used, this problem would be underconstrained; even with a priori, the annual measurements provide little insight into the seasonal pattern of the fluxes. For these reasons this case has not been used so far in published studies and will not be addressed in this study either.

[9] There has been a debate in the scientific community about which of the three inverse approaches used so far (T1a, T1m, and TDm) is the most reliable for predicting long-term flux averages, given the actual CO<sub>2</sub> measurement database and the strengths and weaknesses of our current three-dimensional (3-D) transport models. One view is that errors in the transport models are likely to have a greater negative impact when comparing to observations at shorter time scales, at which synoptic scale variability and the details of the large seasonal cycles of the fluxes are more pronounced. One could thus argue that the annual data method (T1a) would tend to reduce the uncertainty due to transport errors compared with the monthly data methods (T1m and TDm), since annual diagnostics will average over the monthly varying transport. On the other hand, the flux estimates in the T1a method rely strongly on the time distribution assumed for the a priori fluxes, as noted by *Bousquet et al.* [1999b], and one can question the validity of an inversion that would match only the annual observations without being required to match the seasonal cycle as well. How the annual mean biospheric CO<sub>2</sub> flux should be distributed seasonally, whether during the growing season or during the winter, is largely uncertain. From this point of view the monthly adjustment method (TDm) has the advantage of being rather independent of the seasonal pattern assumed for the a priori sources. The T1m method is an intermediate case. It generally has the advantage of having more data values constraining the inversion than parameters being solved for. On the other hand, this inversion fits the seasonal data using fixed a priori temporal flux patterns that might well be erroneous. Given these considerations, the choice of the most robust time resolution remains unclear and tightly related to the transport model and the a priori fluxes that are used. In this study, we will

**Table 2.** Spatial Resolution, Wind Fields, Convective Scheme, Interhemispheric Exchange Times and Reference for the Three Models Used in the Inverse Comparison<sup>a</sup>

Model	Resolution (lon × lat × lev.)	Wind	Convection	Interhemis $\tau$		References
				Surface	Global	
TM2	7.5° × 7.5° × 9	ECMWF(90)	Tiedke (89)	1.56	1.10	<i>Heimann et al.</i> [1989]
TM3	5° × 4° × 19	ECMWF(90)	Tiedke (90)	1.83	1.18	<i>Heimann et al.</i> [1995]
GCTM	2.4° × 2.4° × 11	GCM	on-line	1.76	0.82	<i>Mahlman et al.</i> [1978]

<sup>a</sup>The exchange times are calculated from the fossil simulation of the TRANSCOM 1 experiment [Law et al., 1996] and are measured in years. Surface values correspond to the use of only the 2-D surface field to compute  $\tau$ , while global values make use of the 3-D field.

compare the differences in the estimated fluxes obtained using the T1a, T1m, and TDm time resolution to the differences caused by the transport models and spatial discretization assumed. This study extends the work of *Peylin et al.* [1999] and *Law and Rayner* [1999] and establishes a framework for comparing inversions using different time resolutions and transport models. The TransCom 3 inter-comparison (available at <http://transcom.colostate.edu/>) will extend this work with more models.

[10] The choice of a priori uncertainties for the measurements and the a priori fluxes ( $R^o$  and  $P^b$  in equation (1)) requires particular attention. For a relevant statistical comparison of the three time resolution (T1a, T1m, and TDm) we need to ensure that the relative weight between the measurements and priors as a whole is the same in the cost function for the three cases. In order to fulfill this constraint, we use the hypothesis of random and independent errors to set the values in  $R^o$  and  $P^b$ . We define monthly errors for both quantities and then sum them in a root-mean-square (RMS) sense to compute the annual errors (see section 2.3).

## 2.3. Components of the Inversions

### 2.3.1. Atmospheric Transport

[11] We use three different transport models, TM2, TM3, and GCTM, to calculate the CO<sub>2</sub> concentrations at each station that result from each source scenario (we call these maps the response functions). Table 2 summarizes the main characteristics of these models. All three models are off-line 3-D atmospheric tracer transport models driven by meteorological fields derived from the European Center for Medium Range Weather Forecast (ECMWF) for TM2 and TM3 and from a parent General Circulation Model for GCTM. The horizontal and vertical resolutions are different between the three models, GCTM having a much finer grid in the horizontal than TM2 and TM3, and TM3 having the greatest vertical resolution (19 levels). Vertical convective and diffusive transport are computed at all levels in each model.

[12] These models have participated in phases I and II of TransCom, a model intercomparison experiment based on fossil fuel CO<sub>2</sub> emissions and annually balanced biospheric CO<sub>2</sub> fluxes [Law et al., 1996], and SF<sub>6</sub> fluxes [Denning et al., 1999]. (Note that the phase I results for TM3 were run afterwards and reported by *Bousquet* [1997].) The interhemispheric exchange time ( $\tau$ ) computed with a fossil fuel source quantifies the global north to south mixing across the three models (Table 2) for this tracer. The value of  $\tau$  defined using surface concentrations shows that of the three models TM2 has the shortest interhemispheric mixing for the lower atmosphere, and TM3 has the longest. When computed using the full 3-D concentration field, the  $\tau$  values indicate

that GCTM has the fastest exchange time. For the inversion problem addressed here the first measure is more relevant, since most of the CO<sub>2</sub> measurement sites are at the surface. The comparison with the neutral, seasonal biospheric source used in TransCom 1 indicates that TM3 and GCTM produce a large positive south to north latitudinal CO<sub>2</sub> gradient (the so-called “rectifier effect” [Keeling et al., 1989; Denning et al., 1995]), while TM2 produces nearly no gradient. Overall, the TM2, TM3, and GCTM models represent a relatively wide range of transport characteristics (especially in terms of the magnitude of the rectifier) by comparison with the range of models that participated in TransCom. One can thus expect that the inverse fluxes from these three models will account for much of the range of uncertainty that would be contributed by the transport of the models that participated in the TransCom simulations.

### 2.3.2. Atmospheric CO<sub>2</sub> Data

[13] We use measurements of atmospheric CO<sub>2</sub> made at many locations by different networks, smoothed in time, and compiled into a global database [GLOBALVIEW-CO<sub>2</sub>, 1999]. From this database we choose only the stations that took data over most of the 1990–1994 period. Note that this was a period with an abnormally low CO<sub>2</sub> accumulation rate in the atmosphere ( $\sim 1.2$  ppm yr<sup>-1</sup> versus 1.63 ppm yr<sup>-1</sup> for the last 20 years). We excluded some of the Pacific and South China Sea shipboard cruise data, since many of these sites are located very close together (within the same model grid box) and since their time series are defined with a rather small number of flask measurements. Including all of them would overemphasize the atmospheric constraint in those zones. We also excluded two continental sites, Baltic Sea (BAL) and Monte Cimone (CIM) in Italy, as they are not well represented by the coarse resolution of two of the transport models that we use. Those two sites are large outliers from the marine zonal mean reference curve at northern midlatitudes [Masarie and Tans, 1995]. The positions of the 46 sites that we did choose to use are given in Figure 2.

[14] All the inversions performed in this study assume that the seasonal cycles of the estimated fluxes repeat year after year across the data span. We thus define a “climatological” CO<sub>2</sub> time series by fitting the data at each station to a “smooth time series” consisting of an annual mean value, a global trend identical at all sites, and a mean seasonal cycle that repeats for each year [Thoning et al., 1994]. The monthly data error ( $R_{mon,i}^o$ ) is defined at each station,  $i$ , as the standard deviation of all residuals between the raw flask data and the “smooth time series.” For the annual data method (T1a) we derive the errors in the annual mean concentration ( $R_{ann,i}^o$ ) from the errors in the monthly fluxes ( $R_{mon,i}^o$ ) by assuming they are all independent and by

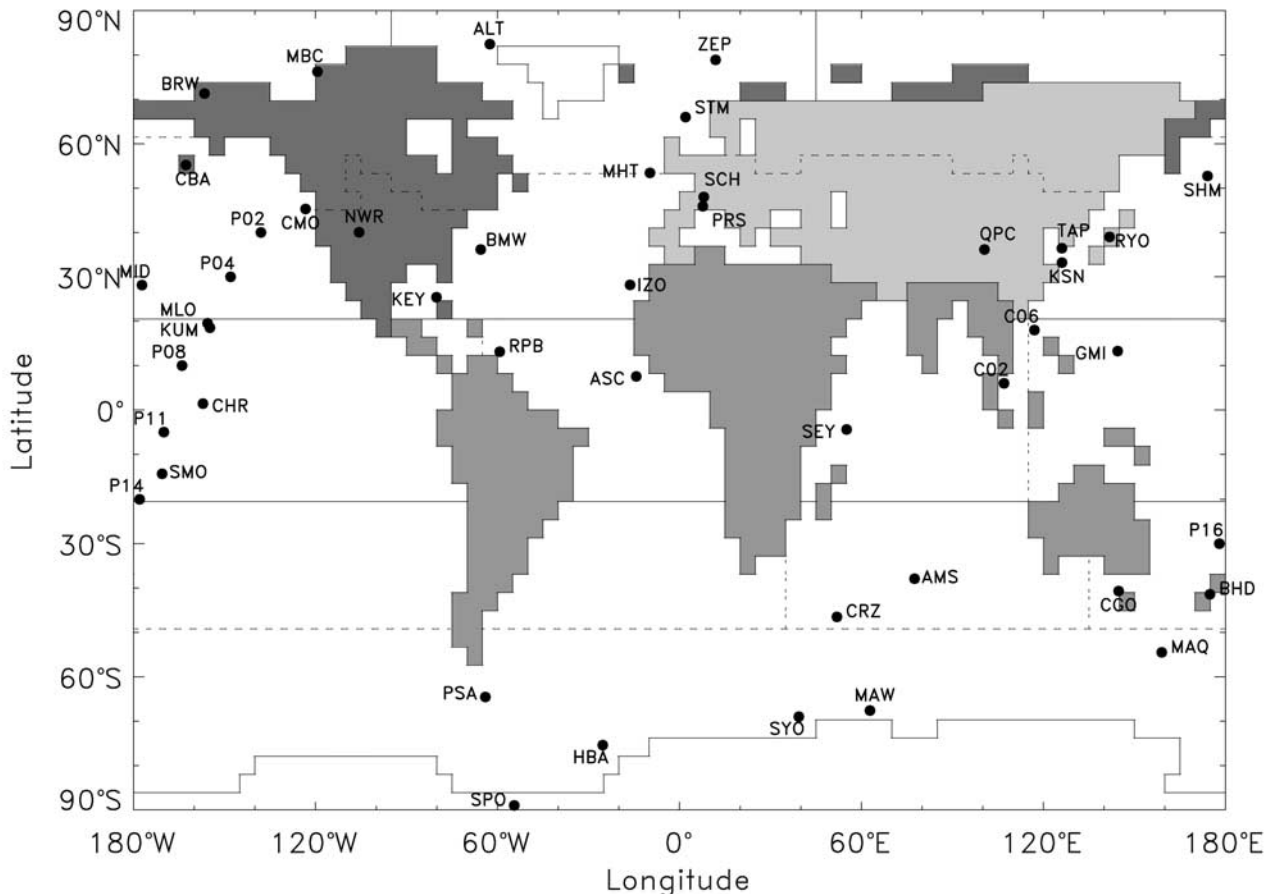


**Figure 2.** Map of the different regions used in the inversions: three land regions in gray (North America, Eurasia, tropics) and four oceanic regions separated by solid lines (North Pacific, North Atlantic, tropics, southern extratropics) for the 7-regions case. The dotted lines figure the division for the 12-regions case (boreal and temperate North America, boreal and temperate Eurasia, tropical America and Africa, Austral-Asia, arctic North Atlantic, temperate North Atlantic, tropical ocean, temperate southern oceans and the southern ocean) and the 17-regions case (same as the 12-regions cases with tropical America and Africa split into two parts, the tropical oceans split into three parts, and the temperate southern oceans split into three parts). The location and acronyms of the stations used in this study are also shown.

summing them in an RMS sense (using the formula  $V[(\sum_{i=1}^{12} X_i)/12] = 1/12 \times V[X]$ , where  $V[\cdot]$  is the variance operator and  $X$  is a random variable) so that

$$R_{ann,i}^o = R_{mon,i}^o / \sqrt{12}. \quad (2)$$

The monthly errors for all sites are given at the bottom of Figure 11.

### 2.3.3. A Priori Flux Scenarios and Spatial Resolution

[15] We specify the following CO<sub>2</sub> sources and sinks (Table 3):

1. The first source is Fossil fuel emissions (FOS). We use the spatial distribution of the annual source compiled by *Andres et al.* [1996] scaled to a global total of 6.1 GtC yr<sup>-1</sup> for the period 1990–1994. We presubtract the resulting concentration at each site from the CO<sub>2</sub> measurements, since this fossil fuel CO<sub>2</sub> source is known much more accurately than the other flux terms.

2. The second source is ocean net flux (OCE). We use the spatial and temporal patterns of the air-sea exchange as

compiled by *Takahashi et al.* [1997]. *Takahashi et al.* [1997] used extrapolated and interpolated  $\Delta p\text{CO}_2$  data and the gas exchange formulation of *Wanninkhof* [1992]. The more recent *Takahashi et al.* [1999] ocean flux distribution includes new measurements of  $\Delta p\text{CO}_2$  in the southern ocean and gives a global ocean sink of  $-2.2 \text{ GtC yr}^{-1}$ . We have scaled the *Takahashi et al.* [1997] spatial flux patterns by region to the regional magnitudes given by *Takahashi et al.* [1999] but modified slightly to give a global ocean sink of  $-2.0 \text{ GtC yr}^{-1}$ . We choose an annual a priori uncertainty ( $P_{ann,i}^b$ ) of  $1.0 \text{ GtC yr}^{-1}$ , identical for all basins. We define the monthly a priori errors ( $P_{mon,i}^b$ ) in GtC month<sup>-1</sup>, by assuming that the errors in the monthly fluxes are all random and independent, as

$$P_{ann,i}^b = P_{mon,i}^b \times \sqrt{12}. \quad (3)$$

3. The third source is biotic gross fluxes. For the TM2 and TM3 transport model cases we use the biotic gross

**Table 3.** Sources Used in the Inversions of Atmospheric CO<sub>2</sub> Observations: Photosynthetic and Respiratory Exchanges (GPP/NPP and RES/RES<sub>h</sub>), Air-Sea Fluxes (OCE), and Fossil Fuel Emissions (FOS)<sup>a</sup>

Type of Source	Number of Regions			Annual Flux (GtC)	Annual Uncertainty	References
	R17	R12	R7			
GPP/NPP	7	6	3	-100/-49	50%	<i>Denning et al.</i> [1996]/ <i>Potter et al.</i> [1993]
RES/RES <sub>h</sub>	7	6	3	100/49	50%	<i>Denning et al.</i> [1996]/ <i>Potter et al.</i> [1993]
OCE	10	6	4	-2.0	1.0 GtC/reg.	<i>Takahashi et al.</i> [1999]
FOS	1	1	1	6.1	presubtracted	<i>Andres et al.</i> [1996]

<sup>a</sup>Inversions R7/R12/R17 refer to different regional segmentation of the sources (the number of regions is indicated). The global annual flux is in GtC yr<sup>-1</sup>, the annual a priori uncertainty is expressed either as a percentage of the annual flux or as a mean value per region, and references for the space-time flux patterns are indicated.

fluxes of photosynthesis and respiration (GPP/RES) from the simple biosphere (SiB2) land surface model [Denning et al., 1996]. For the GCTM model cases we use the net primary production and heterotrophic respiration (NPP/RES<sub>h</sub>) given by the Carnegie Ames Stanford Approach (CASA) model [Potter et al., 1993]. The response functions for these fluxes are the same ones used by us in previous studies (Bousquet et al. [1999a] and Peylin et al. [1999] for TM2 and TM3 and Baker [2001] for GCTM). The use of different biotic flux scenarios allows us to partially account for uncertainties in the spatial distribution of the biospheric sink. Both the SiB2 and CASA models are based on vegetation indexes retrieved from satellite measurements, but they use very different parameterizations to compute photosynthesis and respiration, as well as different climatic variables. CASA uses a “light use efficiency” formulation to convert the solar energy flux absorbed by plants into net primary productivity [Potter et al., 1993]. SiB2 uses photosynthesis equations originally developed at the leaf scale, scaled up to the canopy level. The SiB2 model predicts gross carbon assimilation ( $\sim$ GPP) [Sellers et al., 1996] as a function of the climate simulated in the Colorado State University General Circulation Model (CSU-GCM) [Denning et al., 1996]. The resulting Net Primary Production fields have been compared with those from 15 other land biosphere models in the “Potsdam NPP comparison” [Cramer et al., 1999]. The spatial distribution of the NPP given by SiB2 and CASA are quite similar, compared with the full range spanned by the 17 models. On the other hand, they differ significantly in the temporal distribution of the Northern Hemisphere NPP, with a more pronounced seasonality in SiB2 than in CASA. In the inversions the annual a priori errors are set fairly loosely to values that are 50% of the gross fluxes (GPP/RES for TM2 and TM3 and NPP/RES<sub>h</sub> for GCTM). The annual uncertainty is split evenly across the 12 months by dividing it by  $\sqrt{12}$  (equation (3)).

[16] In calculating the response functions, the a priori fluxes of each source type are gridded on a global map at the resolution of the transport model, with a time resolution of one month, then used as a flux boundary condition at the surface as the transport model is run forward in time. This is done separately for a number of large emission regions, depicted in Figure 2. The flux estimate is given as a flux magnitude multiplying the temporal and spatial pattern assumed inside the corresponding emission region. There is currently a debate about whether one should use a large number of regions

to recover more information from the data and be less sensitive to the a priori spatial patterns or use a small number of regions to avoid underdetermined sources given the sparseness of the present atmospheric network. Note that the computational cost of defining the response function for a large number of regions can also be prohibitive. One naturally incurs larger estimation errors when solving for smaller regions, but when these regions are grouped together, anticorrelating errors cancel out to some extent, leaving smaller errors for the larger regions. Kaminski et al. [2001] have shown that the degree of aggregation can cause large differences in the estimated fluxes and that significant biases might occur when solving for large regions, given the high uncertainty in the shape spatial patterns assumed inside them. Kaminski et al. [2001] referred to this as “aggregation error.” On the other hand, the “estimation uncertainty” obtained, given some random measurement noise and a priori constraint, might also increase with the number of regions solved for.

[17] The debate might also be summarized by the question, How can we best include knowledge on biogeochemical processes and driving factors, which control the mean surface fluxes in an inversion of the atmospheric measurements? Up to now, surface fluxes for large regions have been distributed according to biogeochemical models (SiB2 and CASA for this study) that capture only few possible mechanisms for the CO<sub>2</sub> land uptake. A possible improvement would be to increase the number of regions solved for and set up correlations between errors on the fluxes of those regions. These correlations should be defined on the basis of our imperfect knowledge of the link between regions of similar behavior in terms of CO<sub>2</sub> uptake or release (i.e., correlation lower than 1). Another issue to consider is that the current measurement network permits robust flux estimates (i.e., with low random estimation error) at only the larger spatial scales. Thus there is probably an optimal number of regions to solve for that minimizes the sum of the “aggregation error” (lower at high resolution) and “estimation uncertainty” (lower at low resolution).

[18] In this study, as a first step, we investigate the influence of the choice of only a few particular spatial resolutions. We thus performed the inversions solving for the following number of land/ocean regions: 3/4 (the “R7” case), 6/6 (“R12”), and 7/10 (“R17”). Figure 2 displays the boundaries of these different spatial aggregations. Note, however, that because we use the response functions of previous studies, the regional boundaries of

the GCTM model are slightly different than those for TM2 and TM3 (differing by  $<5^\circ$  in latitude or longitude). As part of this study, we also include results for the R12 and R17 runs summed to the 7 regions used in the R7 runs.

### 2.3.4. Additional Constraints

[19] Several additional constraints have been added to the inverse calculations. First, for the annual data method (TIa) we constrain the total land/ocean CO<sub>2</sub> uptake to the average value implied by the difference of the fossil fuel input rate and the atmospheric increase rate for 1990–1994:  $1.6 \pm 0.01 \text{ GtC yr}^{-1}$ . This constraint on the sum of all sources is needed not only for the TIa method that does not contain information on the yearly atmospheric increase rate but also for the monthly data methods (TIm and TDm), since part of this increase is missing on the 12 monthly data (first half of January and second half of December). Second, we require that the GPP and RES fluxes roughly balance across the year for the TM2 and TM3 cases (and similarly with NPP and RES<sub>*h*</sub> for GCTM). Their annual sum is forced towards  $0.0 \pm 2.0 \text{ GtC yr}^{-1}$  over each region, except for the tropical regions, where the error is set at a tighter  $\pm 1.0 \text{ GtC yr}^{-1}$  to avoid some large dipoles between the poorly constraint tropical regions, following the approach of *Bousquet et al.* [1999a]. These uncertainties permit some imbalance between the two gross fluxes, resulting in a net source (GPP < RES) or sink (GPP > RES) of carbon. They are identical between the different cases to allow direct comparison of the results.

[20] Third, independent studies using O<sub>2</sub>/N<sub>2</sub> and  $\delta^{13}\text{C}$  atmospheric measurements have been able to partition the global carbon uptake between land and ocean [*Ciais et al.*, 1995; *Keeling et al.*, 1996; *Battle et al.*, 1996; *Langenfelds et al.*, 1999]. Recently, *Battle et al.* [2000] summarized these results and inferred an ocean sink of  $2.0 \pm 0.6 \text{ GtC yr}^{-1}$  for the 1991–1997 period using O<sub>2</sub>/N<sub>2</sub> and  $\delta^{13}\text{C}$  measurements from a global network. (Note that the recently released IPCC-2001 report has obtained slightly different estimates.) In order to include such information in the inversions, we have constrained the global annual ocean flux to  $-2.0 \pm \nu \text{ GtC yr}^{-1}$ . The uncertainty  $\nu$  is varied using the values 0.1, 0.3, 0.5, 0.8, 2.0, 4.0, and 100.0  $\text{GtC yr}^{-1}$  in order to test the influence of such a global constraint on the regional partition of the CO<sub>2</sub> fluxes. The case  $\nu = 0.1$  (the tightest constraint) forces the optimized global ocean sink close to the estimated value of  $2.0 \text{ GtC yr}^{-1}$ , while the case  $\nu = 100.0$  (the loosest constraint) corresponds to almost no constraint at all on the sum of all ocean fluxes. We have also included a case where the air-sea flux of each ocean basin is fixed separately to its a priori value given by the “1995” model of *Takahashi et al.* [1999]. Finally, in the monthly adjustment method (TDm), specific constraints are applied in order to avoid unrealistic monthly fluctuation of the source magnitudes over poorly constrained regions. For TM2 and TM3 we impose constraints on the monthly flux differences between consecutive months for each source type, as given by *Peylin et al.* [1999]. For GCTM we use the frequency truncation method of *Baker* [1999] and solve for only half of the resolvable frequencies (giving an effective time resolution of 2 months). These different regularization methods reflect those commonly used in the setups of the TDm time resolution in the Laboratoire des Science du

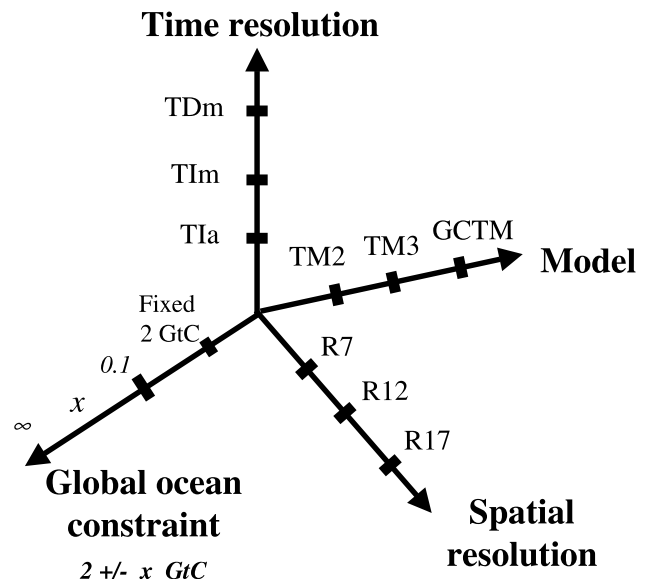


**Figure 3.** Diagram of the varying parameters tested in this inverse experiment. Three models are tested, with three spatial resolutions (7, 12, or 17 regions), three time-resolution methods, and with a global constraint on the ocean flux of varying tightness.

Climat et de L’Environnement (LSCE) group and by *Baker* [2001] at Princeton.

### 2.4. Summary of the Setup for the Inversions

[21] This inverse study is a sensitivity study in which we intend to investigate the influence of the key components of the inversion on the estimated fluxes. Figure 3 summarizes the number of parameters that we varied, along with their assigned values. There are four main axes of variability, including model transport, the form of temporal discretization assumed for the fluxes and the data, the number of aggregated flux emission regions, and the global ocean constraint. Overall, we performed a total of 189 inversions by systematically varying each parameter in Figure 3. Note that we will mainly discuss the 27 inversions corresponding to the global ocean uptake constraint of  $-2.0 \pm 0.8 \text{ GtC yr}^{-1}$ . The 27 inversions include the three different time resolutions (TD/m, TI/m, and TI/a) at three spatial resolutions (R7, R12, and R17) using three transport models (TM2, TM3, and GCTM). For each of these inversions we used the same set of CO<sub>2</sub> measurements. For the a priori fluxes the same temporal and spatial distribution was used for air-sea exchanges, while different ones were used for the land fluxes. Note also that for the TDm time resolution with GCTM we only solve for the sum of NPP + RES<sub>*h*</sub> and not for each flux separately (as in the other methods). The concentrations given by the same fossil fuel emission pattern were presubtracted. In terms of the inverse technique there is only a slight difference between the TM2, TM3, and GCTM models when using the TDm time resolution (owing to the additional constraints noted in section 2.2). Note that the estimated fluxes correspond to the 1990–1994 period, which had an unusually large total CO<sub>2</sub> sink; this should be kept in mind when comparing our results with those of other published studies, such as *Fan et al.* [1998] and *Bousquet et*

**Table 4.** Inversion Results for Transport Models GCTM, TM2, and TM3: Fluxes in GtC yr<sup>-1</sup> in the 7-Region Breakdown

	TM2					TM3					GCTM				
	7	12	17	$\sigma$	$\mu$	7	12	17	$\sigma$	$\mu$	7	12	17	$\sigma$	$\mu$
	<i>North America</i>														
TIa	-1.4	-0.3	-0.2	0.7	-0.7	-1.1	0.0	-0.0	0.6	-0.4	-0.9	-0.1	-0.2	0.4	-0.4
TIIm	-0.3	-1.8	-1.8	0.9	-1.3	-0.6	-1.9	-2.1	0.8	-1.5	-1.4	-1.1	-1.0	0.2	-1.2
TDm	-1.1	-0.0	0.1	0.7	-0.4	-1.0	-0.8	-0.7	0.2	-0.8	-0.8	-0.4	-0.4	0.2	-0.6
$\sigma$	0.6	1.0	1.0	0.8		0.3	1.0	1.1	0.7		0.3	0.5	0.4	0.4	
$\mu$	-1.0	-0.7	-0.6		-0.8	-0.9	-0.9	-0.9		-0.9	-1.0	-0.5	-0.5		-0.7
	<i>Eurasia</i>														
TIa	-0.2	-1.4	-1.3	0.7	-1.0	-1.7	-2.0	-1.9	0.2	-1.9	-0.7	-1.8	-1.7	0.6	-1.4
TIIm	-1.7	-1.5	-1.4	0.2	-1.5	-2.4	-2.3	-2.2	0.1	-2.3	-0.6	-1.5	-1.5	0.5	-1.2
TDm	-1.1	-2.0	-2.0	0.5	-1.7	-2.4	-2.5	-2.3	0.1	-2.4	-1.1	-1.8	-1.8	0.4	-1.5
$\sigma$	0.8	0.3	0.4	0.5		0.4	0.2	0.2	0.3		0.3	0.2	0.2	0.5	
$\mu$	-1.0	-1.7	-1.6		-1.4	-2.1	-2.3	-2.1		-2.2	-0.8	-1.7	-1.7		-1.4
	<i>North Pacific</i>														
TIa	-0.7	-0.4	-0.3	0.2	-0.5	-0.1	-0.1	-0.2	0.1	-0.1	-0.3	-0.0	0.0	0.2	-0.1
TIIm	-0.2	-0.1	-0.1	0.1	-0.1	-0.0	-0.2	-0.3	0.1	-0.2	-0.0	0.1	0.0	0.1	0.0
TDm	-0.3	-0.4	-0.4	0.1	-0.4	0.3	0.2	0.2	0.1	0.2	-0.1	-0.0	-0.1	0.0	-0.0
$\sigma$	0.3	0.2	0.2	0.2		0.2	0.2	0.3	0.2		0.1	0.0	0.1	0.1	
$\mu$	-0.4	-0.3	-0.3		-0.3	0.1	-0.0	-0.1		-0.0	-0.1	0.0	0.0		-0.0
	<i>North Atlantic</i>														
TIa	-0.5	-1.0	-1.2	0.4	-0.9	-0.6	-1.5	-1.3	0.4	-1.1	-1.0	-1.2	-1.2	0.1	-1.1
TIIm	-0.3	0.4	0.3	0.4	0.1	-0.3	0.6	0.7	0.5	0.3	-1.0	-0.8	-1.0	0.1	-0.9
TDm	-0.6	-0.9	-0.8	0.2	-0.7	-0.4	-0.6	-0.7	0.2	-0.6	-1.0	-0.9	-1.1	0.1	-1.0
$\sigma$	0.1	0.8	0.8	0.5		0.2	1.0	1.0	0.7		0.0	0.2	0.1	0.1	
$\mu$	-0.4	-0.5	-0.5		-0.5	-0.4	-0.5	-0.4		-0.5	-1.0	-1.0	-1.1		-1.0
	<i>Tropical Land</i>														
TIa	-0.6	-0.1	-0.2	0.3	-0.3	-0.4	-0.4	-0.1	0.2	-0.3	-0.9	-0.7	-0.1	0.5	-0.6
TIIm	-1.2	-0.3	-0.4	0.5	-0.6	-0.8	-0.1	0.8	0.8	-0.0	-0.5	-0.3	0.2	0.4	-0.2
TDm	-0.1	-0.3	-0.5	0.2	-0.3	-0.5	-0.3	-0.0	0.3	-0.3	-0.6	-0.9	-0.6	0.2	-0.7
$\sigma$	0.5	0.1	0.2	0.3		0.2	0.2	0.5	0.4		0.3	0.3	0.4	0.4	
$\mu$	-0.6	-0.3	-0.3		-0.4	-0.6	-0.3	0.2		-0.2	-0.7	-0.6	-0.1		-0.5
	<i>Tropical Ocean</i>														
TIa	0.7	0.7	0.4	0.2	0.6	0.9	0.9	0.3	0.3	0.7	0.7	0.7	0.1	0.3	0.5
TIIm	0.7	0.7	0.5	0.1	0.7	1.0	1.0	0.3	0.4	0.7	0.6	0.7	0.3	0.2	0.5
TDm	0.7	0.8	0.5	0.2	0.6	0.8	0.7	-0.0	0.5	0.5	0.4	0.7	0.2	0.3	0.4
$\sigma$	0.0	0.0	0.1	0.1		0.1	0.1	0.2	0.4		0.1	0.0	0.1	0.2	
$\mu$	0.7	0.7	0.5		0.6	0.9	0.9	0.2		0.7	0.6	0.7	0.2		0.5
	<i>Southern Ocean</i>														
TIa	-0.9	-1.1	-0.9	0.1	-1.0	-0.6	-0.6	-0.4	0.1	-0.5	-0.6	-0.6	-0.6	0.0	-0.6
TIIm	-0.7	-1.0	-0.9	0.1	-0.8	-0.5	-0.7	-0.8	0.1	-0.7	-0.7	-0.7	-0.7	0.0	-0.7
TDm	-1.0	-0.7	-0.6	0.2	-0.8	-0.5	-0.4	-0.2	0.1	-0.4	-0.5	-0.4	0.1	0.3	-0.3
$\sigma$	0.2	0.2	0.2	0.2		0.1	0.2	0.3	0.2		0.1	0.2	0.4	0.3	
$\mu$	-0.9	-0.9	-0.8		-0.9	-0.6	-0.5	-0.5		-0.5	-0.6	-0.5	-0.4		-0.5

al. [1999a]. The recent studies of Rayner *et al.* [1999], Bousquet *et al.* [2000], and Baker [2001] indeed show large interannual changes in the regional CO<sub>2</sub> fluxes over the 1980–1998 period.

### 3. Results

[22] In this section, we summarize our results by presenting the annual mean regional fluxes averaged over our 27-experiment sample, along with their standard deviation across the sample. We will attempt to explain the differences among the experiments in section 3. Unless noted otherwise, the total ocean uptake was constrained to  $2.0 \pm 0.8$  GtC yr<sup>-1</sup>. For reference the detailed flux results for the 27 experiments are presented in Table 4, in terms of annual mean flux values in the 7-region breakdown. To get the results for all 27 experiments into this common format, the monthly fluxes for the TDm cases were averaged into yearly values and the 12-

and 17-region results were grouped into the 7-region breakdown. We start by discussing the most robust features of the inversion (the global total and the latitudinal breakdown of the fluxes) then we address the least robust features (the land/ocean partitioning of the fluxes and the regional flux distribution in longitude).

#### 3.1. Latitudinal Distribution of Total Flux

[23] Figure 4 gives the total annual land and ocean flux results for three latitude bands and the global total; the total uptake (land + ocean) is also given. The colored bars give the  $\pm 1\sigma$  range of the results in the 27-experiment sample, with the mean value lying in the middle of the bar; the thin lines on the outside give the extreme values from the sample. The total global uptake is estimated with very good precision (within 0.1 GtC yr<sup>-1</sup>) by all experiments, which reflects the use of the additional constraint on the sum of all fluxes, as described in section 2. For the 1990–1994 period

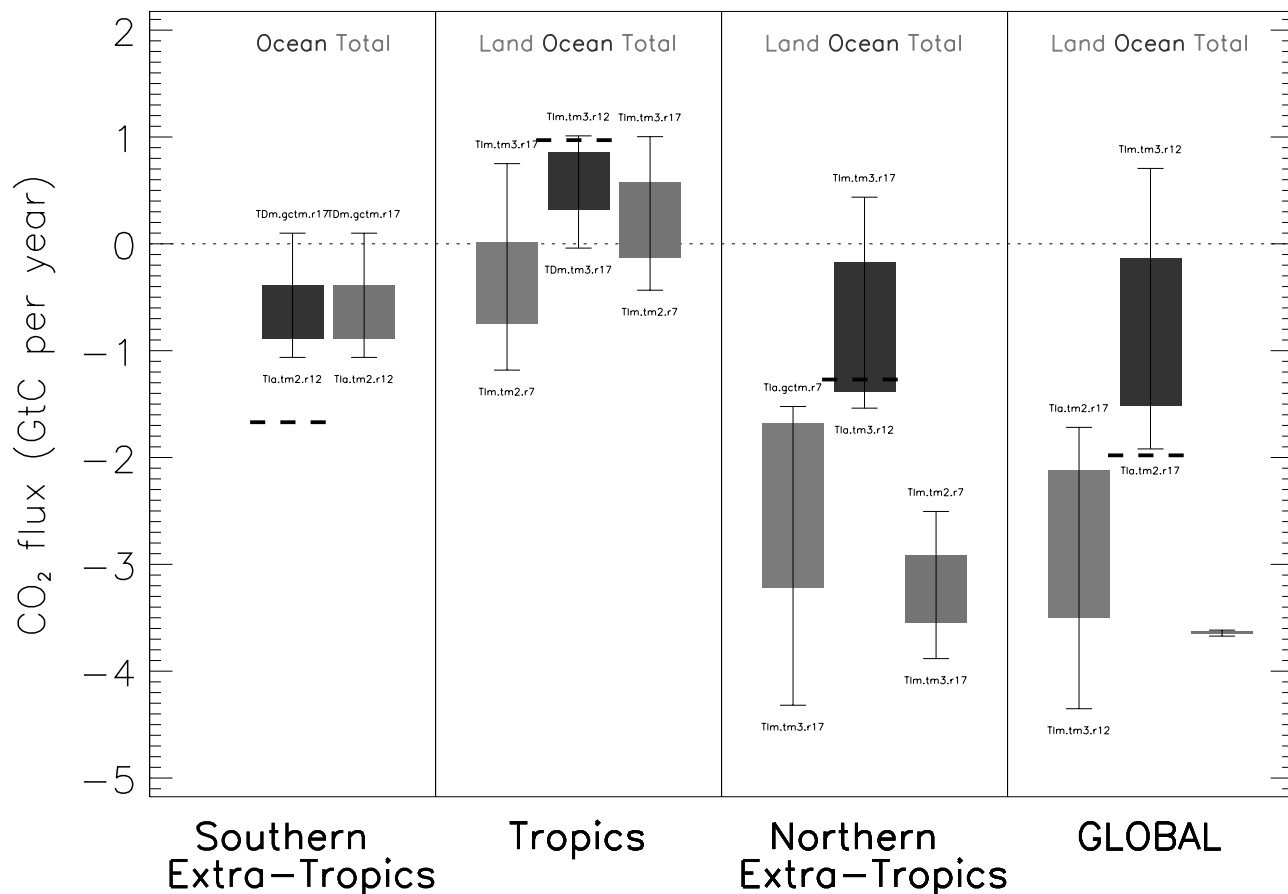


**Figure 4.** Annual land, ocean, and total fluxes from our 27 inversions (3 models  $\times$  3 time-resolution methods  $\times$  3 spatial resolutions) reported for three latitude bands and the global total. The gray bars give the  $\pm 1\sigma$  range of the results, with the mean lying in the middle of the bar. The thin lines on the outside give the extreme values of the 27-experiment sample, along with their acronym (see text for definition). Dashed horizontal lines indicates the ocean uptake estimated by *Takahashi et al.* [1999].

chosen the accumulation rate of carbon in the atmosphere is  $2.45 \text{ GtC yr}^{-1}$  and the fossil fuel emission rate is  $\sim 6.1 \text{ GtC yr}^{-1}$ . These rates imply a total land/ocean carbon uptake of  $3.65 \text{ GtC yr}^{-1}$ , which is much larger than the mean land and ocean uptake for the 1980s of  $1.9 \text{ GtC yr}^{-1}$  [IPCC, 1995]. The increase of global carbon uptake during the early 1990s has been attributed mainly to an enhanced land uptake by *Ciais et al.* [1995], *Keeling et al.* [1996], *Bousquet et al.* [2000], and *Baker* [2001].

[24] The total flux (land + ocean) for each latitude band is also estimated with little scatter across the 27 experiments. A large sink of  $-3.2 \pm 0.3 \text{ GtC yr}^{-1}$  is obtained in the north ( $>20^\circ\text{N}$ ), a small source of  $+0.2 \pm 0.35 \text{ GtC yr}^{-1}$  in the tropics ( $20^\circ\text{N}-20^\circ\text{S}$ ) (the southern land regions are included in this value, as well) and an ocean uptake of  $-0.6 \pm 0.25 \text{ GtC yr}^{-1}$  in the south ( $<20^\circ\text{S}$ ). The above errors correspond to the  $\pm 1\sigma$  range of the 27-experiment sample. A larger uptake is required in the north than in the south in order to match the observed north-south gradient in CO<sub>2</sub> observations. The sum of north + tropics + south must match the observed global trend. As shown in Figure 4, there are also outlying cases that differ substantially from the mean latitudinal values of the full set of inversions. However, some of these outliers can be disre-

garded (see section 4), leading to a smaller overall scatter (see Table 5).

[25] Though not shown in Figure 4, there are systematic latitudinal differences between the results of the three transport models. The differences in the total flux between the northern and southern latitude bands are stable for a given model across the time resolution and spatial resolution axes, averaging  $-2.2 \text{ GtC yr}^{-1}$  for TM2,  $-2.7$  for GCTM, and  $-3.1$  for TM3. Since the extratropical fluxes are the primary ones that drive the interhemispheric gradient in CO<sub>2</sub> concentration (tropical fluxes spreading more evenly across both hemispheres and causing less of a gradient at the surface stations), these north-south flux differences should be fairly well constrained by the observed north-south CO<sub>2</sub>

**Table 5.** Global Normalized  $\chi^2$  Defined as Twice the Cost Function at its Minimum (equation (4)) Divided by the Number of Observations ( $N_{\text{obs}}$ )

	TM2	TM3	GCTM	Mean
Tla	2.0	2.0	2.8	2.3
TIm	1.0	1.6	0.6	1.1
TDm	0.5	0.5	0.4	0.5

concentration gradients. The systematic differences in the north-south flux gradient are thus likely to be due to the transport properties of the individual models themselves, in particular, to the meridional mixing of nonseasonal extratropical sources such as fossil fuel CO<sub>2</sub>, and to the north-south gradient in CO<sub>2</sub> concentration caused by the land biosphere rectification effect. This is discussed further in section 4.

### 3.2. Latitudinal Distribution of Land/Ocean Fluxes

[26] While the latitudinal distribution of the land and ocean flux is fairly robust, the same cannot be said of the apportionment of these fluxes between land and ocean. Figure 4 shows that the global land-ocean partitioning has an uncertainty as large as  $\pm 0.7$  GtC yr<sup>-1</sup> ( $1\sigma$ ). The total ocean flux ranges between  $-1.9$  GtC yr<sup>-1</sup> in the “Tla.tm2.r17” case and  $+0.7$  GtC yr<sup>-1</sup> in the “TIm.tm3.r12” case, even though this quantity was constrained a priori to  $-2.0 \pm 0.8$  GtC yr<sup>-1</sup>. The land uptake varies between  $-4.3$  and  $-1.7$  GtC yr<sup>-1</sup> in the same cases. None of the cases gives a total ocean uptake as large as the current best guess estimates for the 1990s:  $-2.0 \pm 0.6$  GtC yr<sup>-1</sup> from O<sub>2</sub>/N<sub>2</sub> and CO<sub>2</sub> trends [Battle *et al.*, 2000] or  $-2.2 \pm 0.5$  GtC yr<sup>-1</sup> from a suite of ocean models [Orr *et al.*, 2001]. Even if these latter anthropogenic uptakes are adjusted for a preindustrial ocean out-gassing of  $+0.6$  GtC yr<sup>-1</sup> [Sarmiento *et al.*, 2000; Aumont *et al.*, 1999; Sarmiento and Sundquist, 1992], the resulting net ocean uptake of  $\sim -1.6$  GtC yr<sup>-1</sup> barely falls within the extreme range of the inversion results.

[27] Figure 4 gives the latitudinal ocean flux totals. The tropical ocean flux is estimated with little spread at  $+0.6 \pm 0.3$  GtC yr<sup>-1</sup> ( $1\sigma$ ) and is quite close to the Takahashi *et al.* [1999] “1995” model value of  $0.9$  GtC yr<sup>-1</sup>. The northern ocean sink estimate of  $-0.8 \pm 0.6$  GtC yr<sup>-1</sup> is within  $1\sigma$  of the Takahashi *et al.* [1999] value of  $-1.3$  GtC yr<sup>-1</sup>, and this agreement improves when a few outlying runs are removed: Table 5 shows that the scatter in the northern ocean sink results drops when the spurious TIm cases are removed, and the mean sink increases to  $-1.05$  GtC yr<sup>-1</sup> (see the discussion in section 6). The southern ocean uptake of  $-0.6 \pm 0.25$  GtC yr<sup>-1</sup> ( $1\sigma$ ), however, is significantly smaller than the  $-1.7$  GtC yr<sup>-1</sup> “1995” model estimate of Takahashi *et al.* [1999] or even their former “1990” model estimate of  $-1.2$  GtC yr<sup>-1</sup>. Note that the increase in ocean uptake in the “1995” model of Takahashi *et al.* [1999] is due primarily to their inclusion of new data, particularly in the Southern Indian Ocean. In the recent Carbon Model Inter-comparison Project (OCMIP), Sarmiento *et al.* [2000] and Orr *et al.* [2001] have compared the estimates of air-sea CO<sub>2</sub> fluxes from different ocean carbon models for preindustrial times and for the anthropogenic perturbation, respectively. The total uptake for the southern ocean, although highly variable between the ocean carbon models, is on average  $-1.5$  GtC yr<sup>-1</sup>, a larger sink than the inverse estimates.

[28] A net sink of  $-0.4 \pm 0.4$  GtC yr<sup>-1</sup> ( $1\sigma$ ) is indicated in Figure 4 for the tropical land regions, suggesting that any carbon released by deforestation there has been compensated for by regrowth. There are no new deforestation estimates for the 1990s, but it is reasonable to assume that these figures have not changed strongly on the scale of our large regions from one year to the next [Houghton, 2000].

With an estimated deforestation source for the 1980s in the range of  $+0.6$  to  $+2.5$  GtC yr<sup>-1</sup> our inversions suggest a net tropical land uptake in the range of  $-1.0$  to  $-2.9$  GtC yr<sup>-1</sup>. The land sink north of 20°N is highly uncertain, but at  $-2.4 \pm 0.8$  GtC yr<sup>-1</sup> ( $1\sigma$ ), it is also a key term in the total carbon budget. Recall that over the 1990–1994 period, an anomalously large land/ocean carbon uptake apparently occurred, compared with the mean uptake over the last 2 decades. Our inversions allocate this increase in the sink both to the tropical land and to the Northern Hemisphere land, with a large spread in the north (ranging from  $-1.5$  GtC yr<sup>-1</sup> in the “Tla.gctm.r7” case to  $-4.3$  GtC yr<sup>-1</sup> in the “TIm.tm3.r17” case).

[29] The inversions must place more uptake in the north than the south so that the modeled north-south CO<sub>2</sub> concentration gradient will agree with the observed one. In the 27 experiments shown here this is done mainly by placing a large land uptake in the north but also partially by decreasing the southern ocean sink from the a priori value. The inversions plausibly might have increased the ocean uptake in the north to values greater than the  $-1.2$  GtC yr<sup>-1</sup> a priori of Takahashi *et al.* [1999] instead of placing a large sink over land. This would not only have corrected the north-south gradient, but it would have brought the total ocean uptake more in line with the  $-2.0$  GtC yr<sup>-1</sup> best-guess estimate for that time period [Battle *et al.*, 2000]. Nevertheless, the inversions favored less uptake in the northern oceans, compensated by more uptake in northern lands, giving a total sink in the north of between  $-2.9$  and  $-3.5$  GtC yr<sup>-1</sup> ( $1\sigma$ , Figure 4). This solution must be driven by the need to match longitudinal gradients between stations in the Northern Hemisphere. These longitudinal gradients are responsible for the partitioning of the northern sink between land and oceans.

[30] A positive ocean flux total (indicating out-gassing) is clearly out of line with our understanding of the current carbon cycle, yet quite a few of the experiments run here give positive values (4 out of 27). Three of these outliers are with the TM3 model (one with TM2), and they correspond mainly to the annual adjustment/monthly data (TIm) time resolution (three cases out of four). This suggests that in inversions of this sort, CO<sub>2</sub> concentration measurements alone are not sufficient to allow the land and ocean regions to be distinguished robustly (for the mean fluxes), at least for two of the models used in this study for the given station network. This result is even more striking when one considers that the ocean total was constrained a priori at  $-2.0$  GtC yr<sup>-1</sup> with an error level of  $\pm 0.8$  ( $1\sigma$ ). Recall that this constraint was added in order to include information on the ocean uptake from other sources [Battle *et al.*, 2000; Keeling *et al.*, 1996]. We varied the tightness of this  $-2.0$  GtC yr<sup>-1</sup> total ocean flux constraint to see how much it would affect the ocean/land breakdown (Figure 5). As the constraint was tightened, the inferred southern ocean uptake increased only slightly, while the northern ocean uptake increased substantially, both satisfying the ocean total constraint and helping to match the total north-south gradient. As the northern ocean sink increased, the northern land uptake had to decrease to maintain the northern latitudinal total. Note that the inverted tropical ocean source decreased significantly when the constraint was tightened: this had only a small impact on the interhemispheric CO<sub>2</sub> difference.

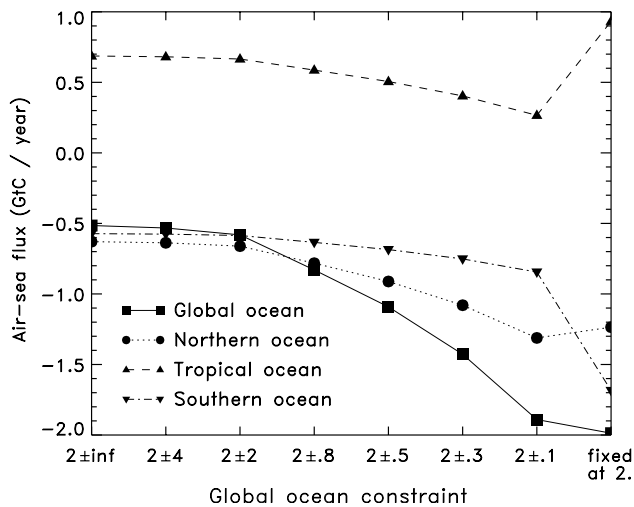


**Figure 5.** Air-sea fluxes for different ocean basins and the total ocean, as function of the tightness of the global ocean constraint:  $-2.0 \text{ GtC yr}^{-1} \pm \epsilon$ , with  $\epsilon$  varying from 0.1 to infinity. In “fixed at 2” case all ocean basins were fixed to the “1995” model fluxes from *Takahashi et al.* [1999]. Fluxes for the 27 experiments were averaged and grouped into the regions defined in the spatial resolution of the “R7” case (see Figure 2).

The ocean total constraint had to be applied at very tight levels before the inversion results approached the  $-2.0 \text{ GtC yr}^{-1}$  target ocean uptake. This suggests that rather than just being highly anticorrelated with the land regions, the ocean estimates are indeed fairly robust. Nevertheless, the global ocean uptake increases from  $-0.5$  to  $-0.8 \text{ GtC yr}^{-1}$  as the constraint is tightened from being infinitely loose to the  $\pm 0.8 \text{ GtC yr}^{-1}$  ( $1\sigma$ ) error level. The case with the tightest error level ( $\pm 0.1$ ) matches the global ocean constraint of  $-2.0 \text{ GtC yr}^{-1}$  but with a large difference for the southern and tropical oceans from their a priori values from the “1995” model of *Takahashi et al.* [1999] (“fixed at 2” case of Figure 5). This trade-off illustrates the inability of the inversions to produce a large southern ocean uptake, at least in the present configuration. This result is, however, similar to most published atmospheric inversions such as *Tans et al.* [1990] and *Gurney et al.* [2002]. The fact that the inversion results give robust global ocean uptakes significantly lower than  $-2.0 \text{ GtC yr}^{-1}$  suggests that a strong preindustrial ocean source may need to be added to estimates of anthropogenic uptake when obtaining total ocean fluxes.

**3.3. Regional Breakdown**

[31] We now consider the estimated fluxes at the continental and ocean basin scales. We present here the fluxes grouped at our coarsest resolution (the 7-region breakdown), focusing in particular on the regions north of  $20^\circ\text{N}$ : North America, Eurasia, the North Pacific, and the North Atlantic. Figure 6 summarizes the results of 27

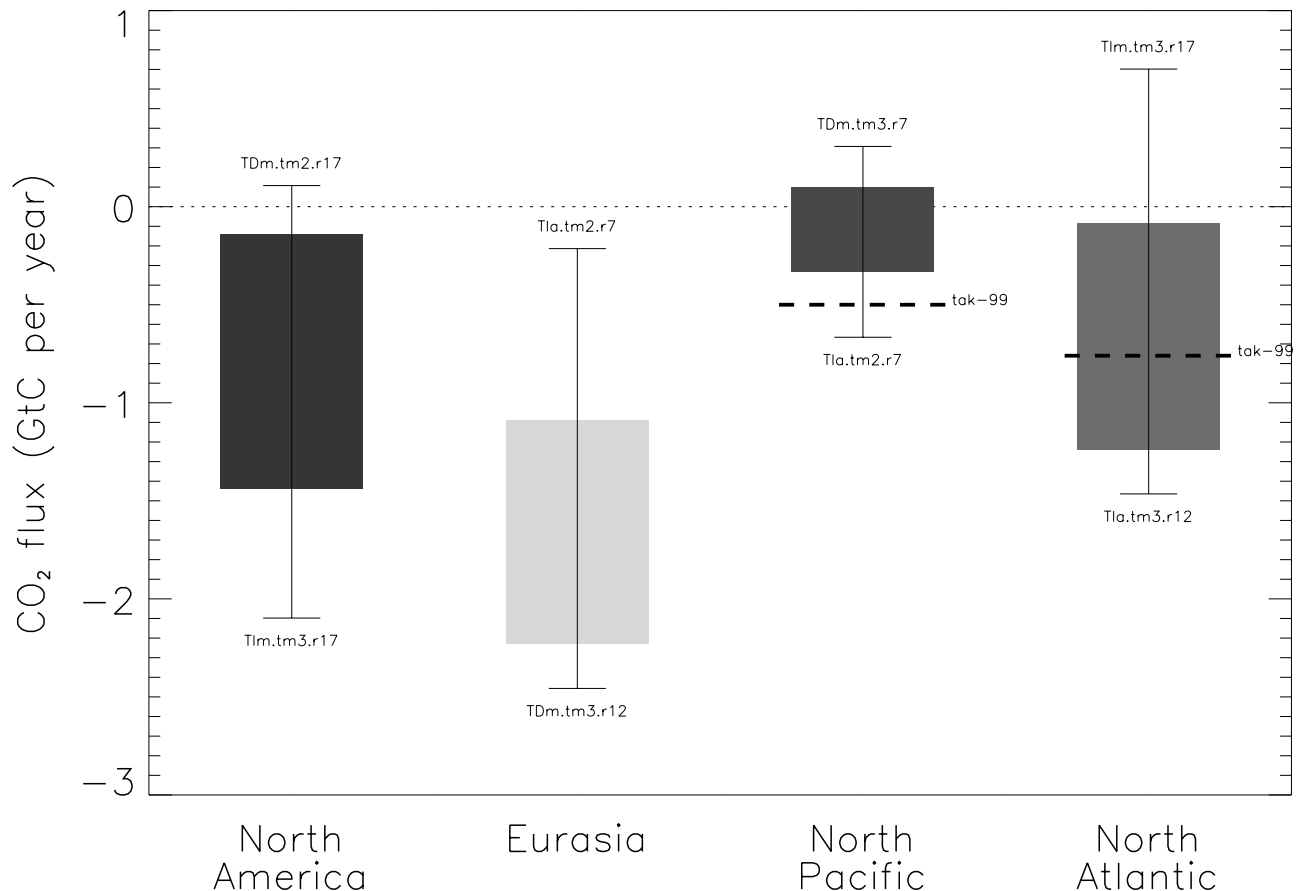


**Figure 6.** Same as Figure 4 but for the four regions of the Northern Hemisphere.

inversions for these 4 regions. The mean partition of the Northern Hemisphere sink by the inversions favors a larger Eurasian CO<sub>2</sub> uptake ( $-1.7 \text{ GtC yr}^{-1}$ ), sinks of similar magnitude in North America and the North Atlantic ( $-0.8 \text{ GtC yr}^{-1}$ ), and a slight sink in North Pacific ocean. Except for this latter region, there is a large spread in the results of the 27 cases (around  $\pm 0.6 \text{ GtC yr}^{-1}$  at  $1\sigma$ ). This uncertainty in the regional partitioning in the north is over twice that of the total (land + ocean) uptake there (Figure 4). In spite of this large regional uncertainty that can be reduced by removing few outlying cases (see section 3.4.1), the inversions suggest that there is more uptake in Eurasia than in North America for the 1990–1994 period. This difference is significant at the  $1\sigma$  level of the systematic errors given in Figure 6 but becomes somewhat less certain if the random errors estimated by the inversion itself are added to these systematic errors (see the discussion of errors in section 3.4).

[32] Much of the regional uncertainty, however, is due to large anticorrelations between the fluxes for North America and the North Atlantic in just 4 of the 27 cases: TIm.tm2.r12, TIm.tm2.r17, TIm.tm3.r12, and TIm.tm3.r17 (see Table 4). These four cases appear as the outliers in the upper left-hand corner of Figure 7, which is a scatter plot of the North American versus North Atlantic fluxes for the 27 cases. If we group these two sets of results separately, their sum can be estimated to within  $0.3 \text{ GtC yr}^{-1}$  ( $1\sigma$ ). This indicates that the stations that we used are unable to fully separate North America and North Atlantic mean fluxes, at least when using the annual adjustment/monthly data (TIm) method with the TM2 and TM3 models (the four outliers). Note in Figure 7 that the other time resolutions (Tla and Tdm) also produce anticorrelation between North America and the North Atlantic fluxes but to a much lesser extent (see section 3.4.2). Figure 7 shows the uptake from the “1995” model of *Takahashi et al.* [1999] for the North Atlantic as a horizontal dashed line. Note that many of our inversion results deviate substantially from this *Takahashi et al.* [1999] North Atlantic estimate, particularly the four outliers mentioned above, which are unlikely to be correct. We shall return to a discussion of these later in the paper.

[33] On the other hand, the estimated flux over the northern Pacific basin appears to be “robust,” with a standard deviation of  $0.2 \text{ GtC yr}^{-1}$  (Figure 6). This result probably reflects the presence of many sites within or at the border of the basin (10 out of 46), ensuring that the fluxes from this region are well observed. Also, the spatial pattern of the surface fluxes over the North Pacific, with uptake in the northwest part and out-gassing in the southeast nearly cancelling each other out in the sum, probably prevents the inversion from estimating large corrections there: Any overamplification of the dipole pattern in the fluxes would be sensed easily at the measurement sites and prevented if not compatible with the data. This observation highlights the problem of having fluxes of both signs within a region, a situation that is more likely with large regions. Note that we did not split the northern Pacific basin into two parts, as we kept the “response function” identical to that of the previous *Baker* [1999, 2001] studies.

[34] According to this study, the longitudinal breakdown of the mean net fluxes in the northern regions is much less

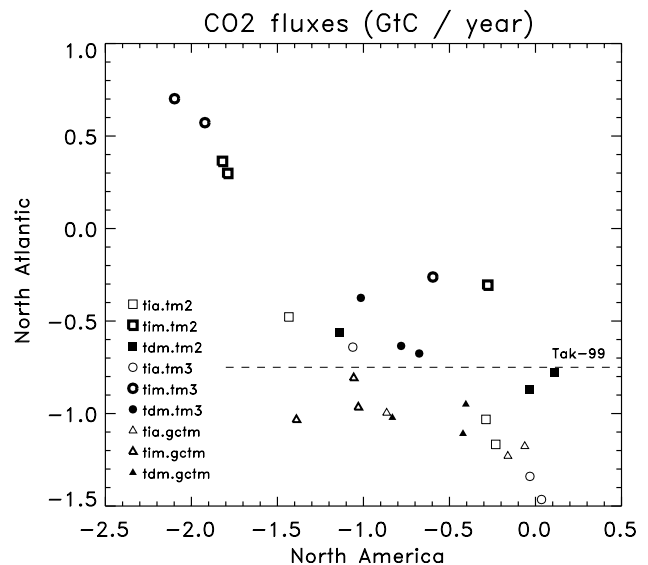


**Figure 7.** Annual CO<sub>2</sub> fluxes for North America versus North Atlantic, as estimated in the 27 inversion cases. The 7, 12, and 17 regions inversions show the same symbols.

robust than the latitudinal totals. This is true both when all 27 sets of inversion results are used to calculate the spread (Figure 6) and when the outlying TIm results are thrown out (Table 5). The range spanned by the 27 estimates is large enough to include most of the recent synthesis inversion results presented in Table 1. The results of *Fan et al.* [1998], who estimated a sink of  $-1.7 \pm 0.5 \text{ GtC yr}^{-1}$  in North America using the equivalent of our Tla approach (with land regions equivalent to our 7-region case, two different estimates of the air-sea flux, and two different GCMs) lie at the edge of our  $1\sigma$  envelope, especially when we remove our TIm cases. Note, however, that the North American uptake of  $1.6 \pm 0.6$  that *Fan et al.* [1998] obtained with the model most similar to our GCTM Tla case (GCTM with the air-sea flux of *Takahashi et al.* [1997], which gives  $-0.55 \text{ GtC yr}^{-1}$  for the Atlantic north of  $15^\circ\text{N}$ ) is larger than the North American uptake of  $-0.9 \text{ GtC yr}^{-1}$  we obtain with GCTM in the equivalent Tla case. They differ by  $\sim 1.3$  standard deviations of each other. On the other hand, the *Fan et al.* [1998] GCTM result cannot be directly compared with our Tla.gctm.r7 case because (1) they held the ocean fluxes fixed to the values of *Takahashi et al.* [1997] and only solved for the three land regions, (2) they examined a different period of time (1987–1992), and (3) they used slightly different stations. Given the high sensitivity of the North American flux to the North Atlantic flux suggested by Figure 7 for the GCTM cases (depicted as triangles), their assumptions (especially hypothesis 1) may have had a large impact on their estimated fluxes for the northern lands. Note, in particular, that the North Atlantic uptake determined in our Tla.gctm.r7 case is  $-1.0 \text{ GtC yr}^{-1}$ , as contrasted to the value of  $-0.55 \text{ GtC yr}^{-1}$  specified by *Fan et al.* [1998] based on *Takahashi et al.* [1997]. Further details on this comparison are given by *Baker* [2001]. Although the North Atlantic is one of the places where *Takahashi et al.*'s [1997] fluxes are most tightly constrained by measurements, more oceanic meas-

**Table 6.** Internal and External Flux Estimation Error<sup>a</sup>

Region	Standard Deviation, GtC yr <sup>-1</sup>	
	Internal	External
North America	0.43	0.65
Eurasia	0.38	0.57
Tropical land	0.39	0.38
North Pacific	0.17	0.21
North Atlantic	0.26	0.58
Tropical oceans	0.19	0.27
Southern oceans	0.15	0.25

<sup>a</sup> Internal error as used here is the random estimation error given by the a posteriori flux covariance matrix. External error is the systematic error in the flux estimate across the three axes of variability examined here; it is calculated from the variance about the mean of our 27-experiment sample.

urements there would help to resolve the disagreement with inverse results.

### 3.4. Error and Covariance Estimates

[35] A strength of the synthesis inversion is that it estimates not only the fluxes over each region but also an associated error covariance matrix. The diagonal terms of the covariance matrix give the errors in the regional fluxes and nondiagonal terms give the covariances between different regions. This matrix characterizes random errors in the flux estimate due to the assumed random uncertainties in the observations and the a priori fluxes; these errors will be referred to here as “internal errors.” While these errors vary slightly between the 27 different inversions (3 models  $\times$  3 types of spatial discretization  $\times$  3 types of temporal resolution), we will discuss only their mean values here. Note, however, that the diagonal terms of the covariance matrix do not account for systematic errors (biases and incorrectly modeled correlations in space and time). A portion of these systematic errors can be estimated from the spread in the annual mean flux estimates given by our 27-member sample. We calculate a covariance matrix from the 27 cases as follows. Diagonal terms are the variances calculated from the 27-member sample for each region. Off-diagonal terms are the covariances between the mean fluxes (27) from different regions. This covariance matrix thus summarizes additional uncertainties due to the parameters that we have varied (the three axes of variability); these errors will be referred to as “external errors” (used in Figures 4 and 6). Both standard deviations and correlation coefficients between fluxes for different regions are calculated from these internal and external covariance matrices and compared. These two types of errors (or correlations) can not be strictly added as they are not fully independent (the a priori data error should in principle account for the transport error, as described by *Tarantola* [1987]), but they both need to be taken into account when discussing uncertainties on the flux estimates. The largest error should at least be considered as a lower bound of the “true” uncertainty.

#### 3.4.1. Errors

[36] Table 6 gives the standard deviation of both the internal and external errors in the annual mean fluxes in the 7-region breakdown, averaged across all 27 experiments. In general, external errors are significantly larger than internal errors, especially for those northern regions whose fluxes have the largest variability among the experiments. This result suggests that there are still large uncer-

tainties associated with the main components of an inversion (the transport model, the spatial patterns of the a priori fluxes, the time resolution) that are not explicitly accounted for in each inverse calculation. However, the different setups that we tested are not likely to be equally valid (see section 3.4.2) so that the estimated external error should be conditional to the likelihood of choosing valid setups. As with the internal errors, the external errors tend to be larger for the land regions than the ocean regions, which are better constrained by the present atmospheric measurement network.

[37] Since the external errors are so large, one clearly cannot use the internal errors given by the least squares covariance matrix to assess uncertainty of regional fluxes. Rather, one could perform sensitivity tests, examining the sensitivity of the inversion result to certain key parameters. A Monte Carlo approach could be used to give realistic external error estimates. Then one should consider both the external and internal errors to get a total error for the estimates. Even then, it must be understood that these error estimates will still tend to be too low, since all sources of systematic error will generally not be explored adequately.

#### 3.4.2. Correlations

[38] As mentioned in section 3.4.1, an external flux correlation matrix was calculated from the mean fluxes of our 27-experiment sample, summarizing the anticorrelations between the flux results for the different regions for the 27 inversion results. Table 7 gives this external correlation matrix for the 7-region breakdown, along with a mean internal correlation matrix (calculated from the average covariance matrix for the 27 experiments). These two matrices really summarize entirely different information. The internal correlation matrix tells us how well a given measurement network (along with a given a priori constraint) can distinguish one region from another in the presence of random measurement noise, assuming a perfect model (perfect basis functions: perfect transport and unbiased sampling). The external correlation matrix, on the other hand, tells us how well the regional fluxes can be distinguished in the presence of systematic errors in the model and across three different time resolutions and three spatial resolutions. Negative correlation values indicate that the current inversions assess the sum of the fluxes for each of these pairs of regions more safely than they do the individual fluxes themselves. In such cases an inversion that gives a larger flux in one region will tend to compensate with a smaller flux in the other, thus maintaining the

**Table 7.** Internal and External Correlation Matrices for the Fluxes in the 7-Region Breakdown<sup>a</sup>

Region	NAm	Eur	TrL	NPc	NAt	TrO	SOc
North America	–	–0.21	–0.33	–0.02	–0.79	–0.12	0.36
Eurasia	–0.61	–	–0.22	–0.48	–0.22	–0.05	–0.43
Tropical land	–0.21	–0.20	–	–0.00	0.24	–0.46	–0.21
North Pacific	–0.09	–0.30	0.05	–	–0.05	–0.15	0.57
North Atlantic	–0.53	–0.10	0.11	–0.07	–	0.23	–0.33
Tropical oceans	0.08	0.05	–0.73	–0.05	–0.03	–	–0.36
Southern oceans	0.15	0.13	–0.80	–0.03	–0.09	0.42	–

<sup>a</sup> The internal correlations, calculated from the a posteriori flux covariance matrix, are given in the lower left of the matrix; the external correlations, calculated from the variability across the 27-experiment sample, are given in the upper right.

combined total. On the other hand, positive correlations between regions indicate that the difference in the fluxes is more robust (i.e., the inverted fluxes tend to move together in response to some changing parameters), as is the case, for instance, for the fluxes that determine the interhemispheric concentration differences.

[39] The largest external anticorrelation is at  $-0.79$ , between North America and the North Atlantic. For a statistic with 22 degrees of freedom (i.e., 27 variables minus 2 and minus 3 linked variables) 90% of correlations should fall inside  $\pm 0.43$ . The North America-North Atlantic anticorrelation is thus statistically significant, as can be clearly seen in Figure 7. It is mainly due to the large spread in the inversions done with the annual adjustment/monthly data method (TI<sub>m</sub>), especially with the four outliers as discussed in section 3.4.1. Without these outliers, the external anticorrelation drops to  $-0.46$ , a value very close to the level of significance. Note also that such an anticorrelation computed with only the annual adjustment/annual data method (TI<sub>a</sub>) reaches  $-0.95$ . Such a large value indicates that with only annual data, the actual atmospheric network is unable to fully separate North America and North Atlantic, at least with our three models. All the other external correlations are below or close to the 0.43 significance level except for a  $+0.57$  correlation between the North Pacific and the southern oceans that involves only little external error ( $\sim 0.2$ , Table 6). The external correlations are quite different from the internal ones, as they largely should be if they are reflecting different phenomena. The largest internal correlations are between the tropical land and the southern oceans ( $-0.80$ ) or the tropical oceans ( $-0.73$ ), reflecting the difficulty in distinguishing the tropical land fluxes from the surrounding ocean fluxes with ocean-based measurement sites and strong vertical transport over the tropical continents. Such values are above the  $1\sigma$  significance of 0.58 (with the number of regions as the number of degrees of freedoms). North America and Eurasia are also anticorrelated but only at the level of  $-0.61$  (slightly significant). The internal correlation between North America and the North Atlantic is only  $-0.53$ , indicating that lack of observability is not the main cause of the external anticorrelation computed for these two adjacent regions.

[40] Again, our results highlight the fact that the internal correlations alone are not sufficient to characterize the codependence of the fluxes and that sensitivity studies must also be performed to identify additional anticorrelations due to nonrandom factors, as already pointed out by *Bousquet et al.* [1999b]. Further analysis must be done to separate the contribution of each axis of variability to the overall external correlation, in order to identify the key parameters. This is done in section 4. In the case of North America and the North Atlantic, fitting seasonal data with a fixed seasonal flux pattern (in the TI<sub>m</sub> time resolution) seems to cause the largest differences in the flux results, at least when using the TM2 and TM3 models.

#### 4. Discussion of the Main Results

[41] In this section, we investigate the causes of the large variance seen across our 27 experiments in the flux estimates at the regional continental and oceanic scale. Often, only a small subset of the 27 inversions, corresponding

either to a particular transport model, time resolution, or spatial discretization, is responsible for most of the spread in the results (i.e., large external variance). It is thus important to isolate and discuss such particular cases. The following discussion will investigate successively the three main axes of our ensemble of inversions (transport model, time resolution, and spatial discretization) to determine their relative contribution to the external variance of the regional fluxes. Figure 8 shows, as a summary, the percentage of the total external variance explained by each of the three major axes of variability. In the following subsections, we analyze each of these in turn and discuss Figure 8.

##### 4.1. Transport Model

[42] Differences in atmospheric transport have been suspected to be a major source of uncertainty trying to relate measured concentration of atmospheric trace gases to surface sources [Law *et al.*, 1996; Bousquet *et al.*, 1999b; Law and Rayner, 1999]. In the Intercomparison Transport Experiment (TRANSCOM) 2, GCTM, TM2, and TM3 were all among the models with the slowest meridional mixing rates for SF<sub>6</sub>, a nonseasonal tracer with an emission pattern similar to fossil fuel CO<sub>2</sub> [Denning *et al.*, 1999]. These slow mixing rates give steep north-south gradients in SF<sub>6</sub> that are, however, in rather good agreement with a north-south SF<sub>6</sub> measurement transect taken in 1993 over the Atlantic Ocean [Denning *et al.*, 1999]. Figure 9b shows the simulated annual mean CO<sub>2</sub> concentrations at the monitoring sites (ordered by latitude) resulting from nonseasonal fossil fuel emissions for the three models. TM3 produces a somewhat steeper north-south gradient than the other two models, in good agreement with the interhemispheric exchange time of the models (see Table 2). A systematic difference of  $\sim 1$  ppmv in the north/south gradient for fossil CO<sub>2</sub> occurs between TM3 and the two other models, and large differences of up to 2 ppmv occur among the three models for certain northern extratropical sites. These differences are probably related to the strength of vertical mixing over the continents, the horizontal winds, and the vertical and horizontal resolution of the models. Both GCTM and TM3 give much higher concentrations at KSN, TAP, and SCH, for example, than does TM2. This is because TM2 has a coarser horizontal resolution than the other two and smoothes out the spatially concentrated fossil fuel sources. The result of this is that stations inside the Asian and European input plumes see lower concentrations in the boundary layer than in the case of the more highly resolved models. Moreover, TM2 produces a smaller vertical gradient over northern extratropical source regions than TM3 and GCTM, reflecting its more powerful vertical mixing. This feature likely relates to differences in sub-grid-scale parameterization of vertical transport between the models. Denning *et al.* [1999] gave maps of the surface concentrations of SF<sub>6</sub> and of the zonal mean cross sections of SF<sub>6</sub> produced by these models in the TRANSCOM 2 experiment that further confirm these differences in vertical mixing.

[43] Figure 9c gives a similar latitude plot for the effect of the seasonal part of the land biosphere (the seasonal rectifier effect). In the TRANSCOM 1 simulation, the zonal mean of GCTM was found to give higher surface values in the northern hemisphere than in the southern hemisphere, while

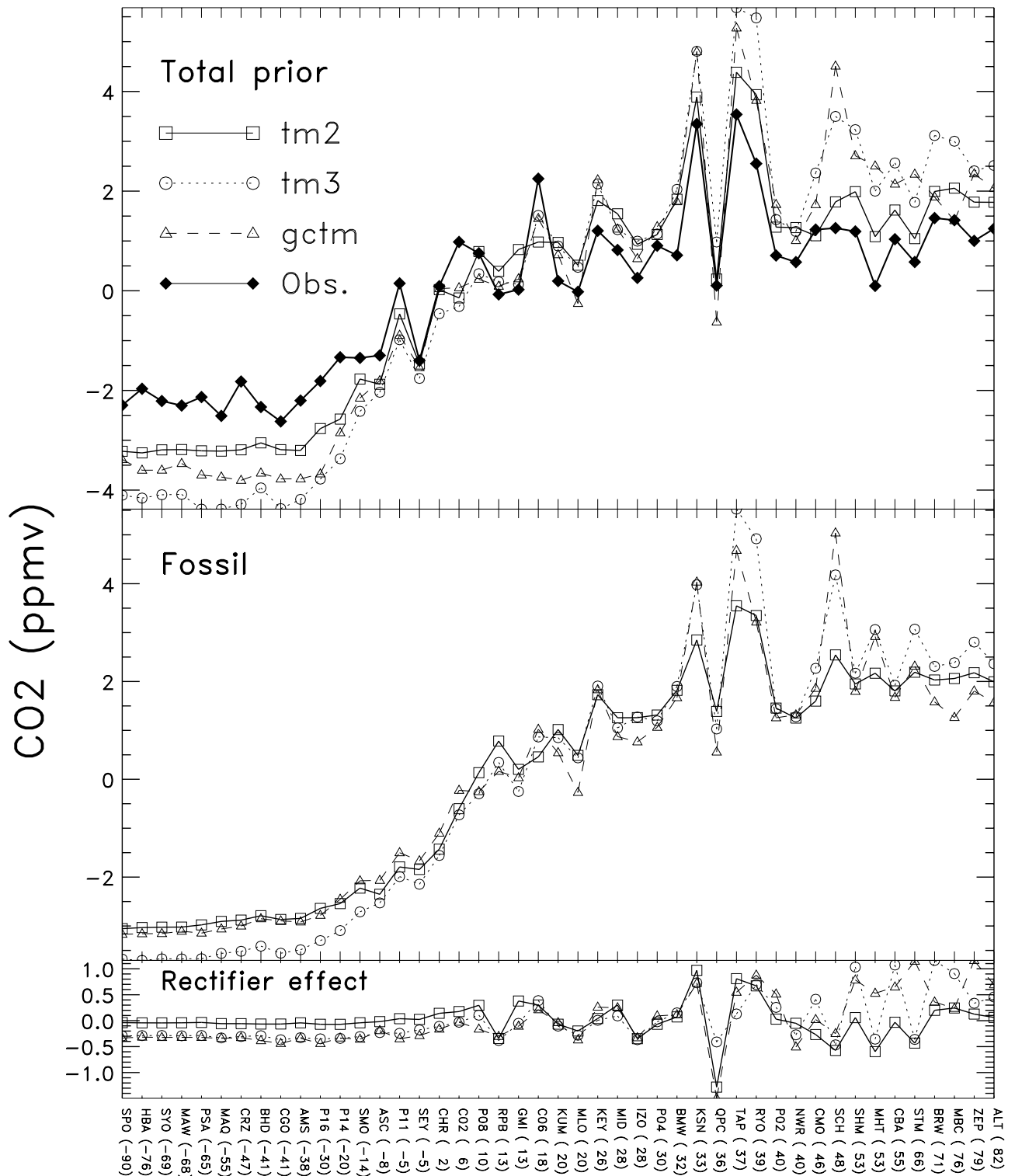
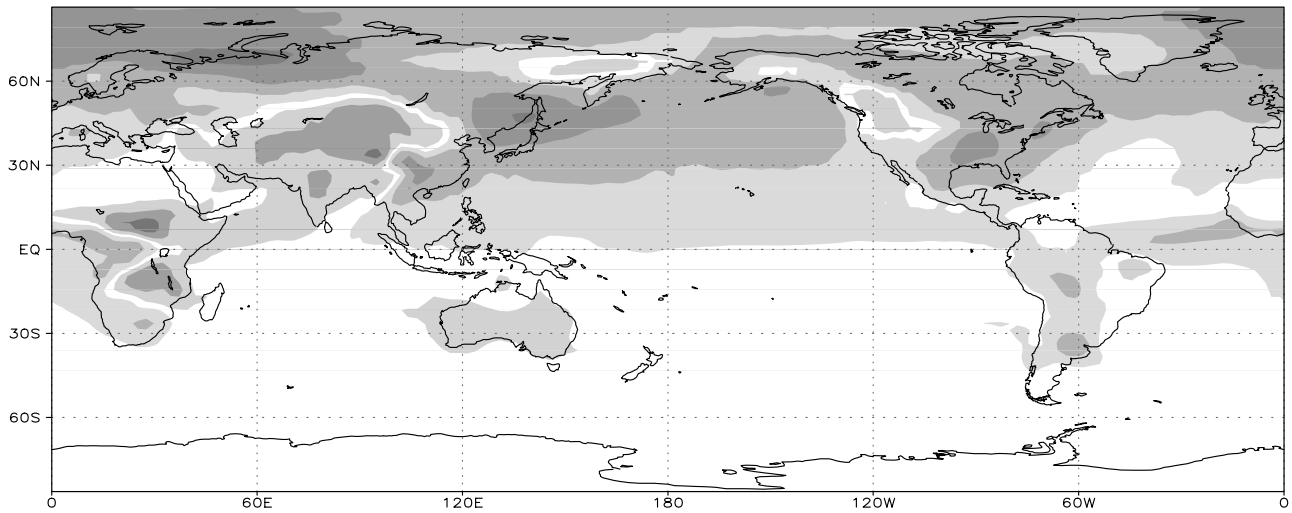
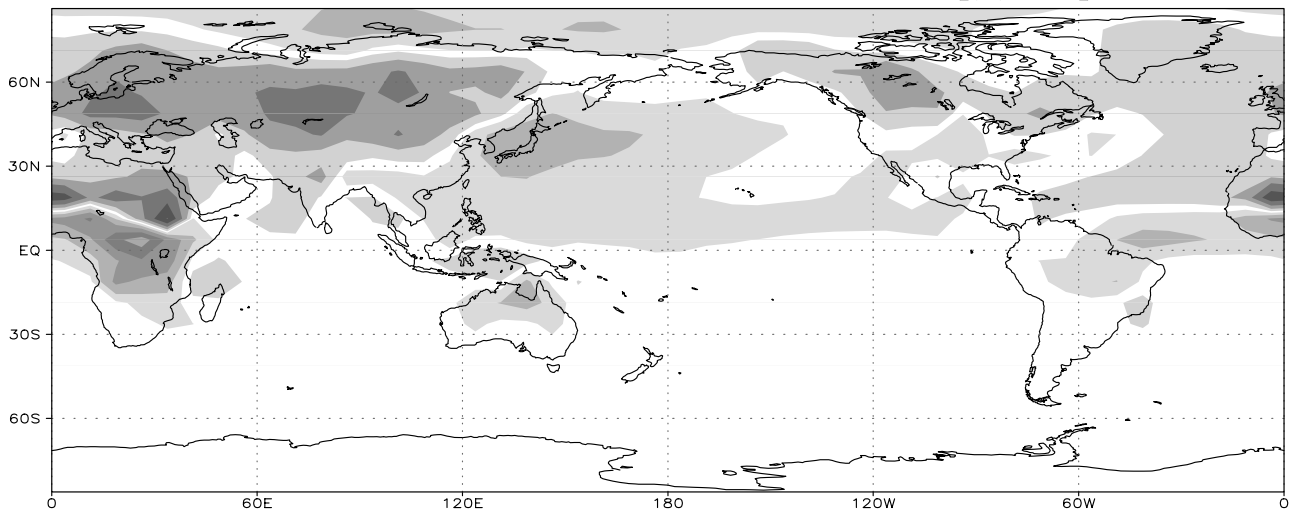


**Figure 8.** Contribution (percent) caused by varying the parameter along each axis (model, time-discretization method, and spatial resolution) to the overall external variance. The latter is calculated from our 27 inversion sample (3 models  $\times$  3 time-resolution methods  $\times$  3 spatial resolutions) and the variance along each axis is defined with three values, each corresponding to the average of the nine inversions performed with this particular parameter held fixed. Note that the sum of the variances along the three axes does not equal the total variance, as the variables are not independent.

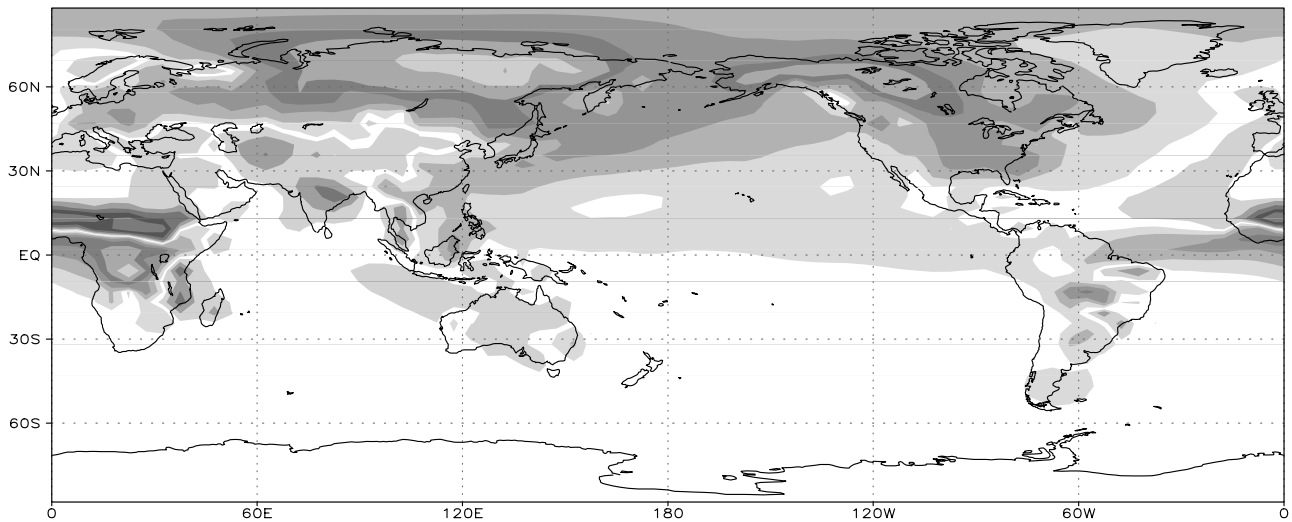
CASA Annual Surface Rectifier, GCTM [ppmv]



SiB2 Annual Surface Rectifier, TM2 [ppmv]



SiB2 Annual Surface Rectifier, TM3 [ppmv]



TM2 showed no such rectification gradient [Law *et al.*, 1996]. This is seen also at the individual sites in Figure 9c. The TM3 model gives an even larger rectification gradient than does GCTM, and much of the variability among the three models occurs in longitude at high northern latitudes. Differences there are of the order of 1 ppmv, and thus slightly lower than for fossil fuel (Figure 9b). The spatial structure of the models' surface rectifier is illustrated in Figure 10. One should recall that part of the differences in rectifier between GCTM and the two other models can be linked to the use of two different models of biospheric flux, CASA versus SiB2. However, as the differences between TM2 and GCTM in Figure 9c are very similar to those reported in the TRANSCOM-1 experiment, in which the biospheric fluxes for the two models were identical, we believe that most of these surface rectifier differences can be attributed to transport differences. Note also that these maps should only be compared in terms of spatial structure and not in terms of the values of the rectifier; they represent the rectifiers of the lowest level of each model, which are at very different heights (70 m in TM3 against 170 m in GCTM and 400 m in TM2). One can clearly see large spatially coherent structures in the rectifier that differ strongly among the three models. The TM3 model presents a strongly positive rectification value over northeast Asia and over northwest America that spreads out over the Pacific Ocean but has nearly no positive rectification over Europe. The rectification pattern in GCTM is more uniform in longitude in the northern extratropics. TM2, on the other hand, tends to produce an annual mean CO<sub>2</sub> deficit over central Asia and Europe compared with surrounding areas. In TM2, increased horizontal transport in winter spreads respired CO<sub>2</sub> out of Eurasia [Ciais *et al.*, 1998] while horizontal transport in summer "concentrates" the summer sink signal over the interior of Eurasia.

[44] Figure 9a displays the latitude plot for the total a priori model concentration, including the effect of fossil fuel, the seasonal land biosphere rectifier, and the Takahashi *et al.* [1999] air-sea fluxes (this last component being rather similar between the three models). The observations averaged across 1990–1994 are also shown. The modeled a priori north-south gradient, which is steeper than the observed one, is corrected in the inversions by adding more of a sink to the a priori in the north than in the south. Some systematic behavior in the flux results of our 27 experiments can thus be directly explained by the transport properties discussed in section 2.3. First, the north-south flux difference for the three models, which was fairly robust for the nine experiments (T1a, T1m, and T1m versus 7/12/17 regions) for each model, agrees well with the sum of the north-south CO<sub>2</sub> gradients caused by fossil fuel burning and the seasonal land biosphere (rectifier) (Figure 9a). TM3 infers the largest flux difference. The fact that it gives the steepest north-south gradient for both fossil fuel and the rectifier suggests that more of a sink is required in the north than the south (to bring this gradient in line with the

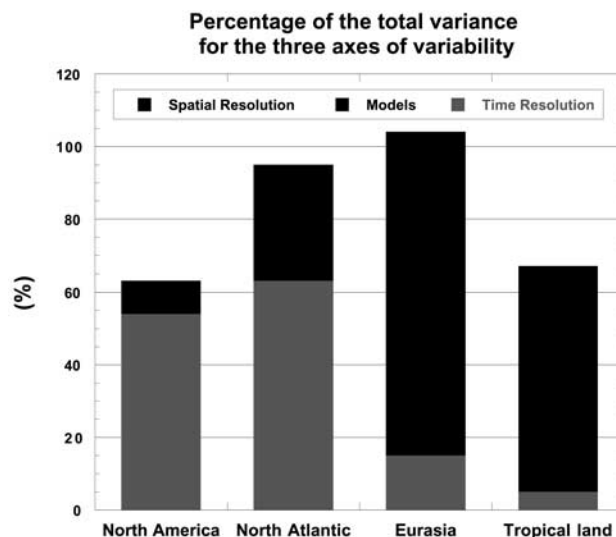


**Figure 10.** The annual mean surface CO<sub>2</sub> concentration (ppmv) produced by the annually balanced land biosphere flux for three biosphere/transport model (lowest level) combinations: CASA/GCTM, SiB2/TM2, and SiB2/TM3. These maps illustrate what Denning *et al.* [1995] call the seasonal land biosphere rectifier effect.

shallower observed CO<sub>2</sub> gradient), although relationships between transport efficiency and inferred fluxes are probably more complex. TM2 had the smallest flux difference, reflecting the fact that it has the shallowest gradient for both fossil fuel and the rectifier. GCTM had an intermediate flux difference, reflecting the fact that it had a fossil fuel gradient and rectifier intermediate between those of TM3 and TM2.

[45] Second, the large uptake in Eurasia inferred by TM3 can be explained by the large positive rectifier pattern generated over that region by that model (Figure 10), directly influencing stations SHM, BRW, and CBA. This points to the importance of longitudinal patterns of the rectifier for the partition of the northern extratropical sink between continents and ocean basins. Rectification pattern differences between models will become even more crucial as new surface data become available in the near future over the northern continents. A better quantification of rectification effects is thus essential before any assimilation of new continental data can be considered robust. Overall, the partitioning of the sink in the extratropical Northern Hemisphere relies on interstation differences of the order of 0.5 to 1.0 ppmv (sites north of 40°N in Figure 9a). However, we see in Figure 9 that the intermodel differences for these stations are of this order or larger for both the fossil fuel and rectifier signals; this represents a severe constraint for the actual inversion.

[46] The contribution of transport uncertainties to the overall external variance of the fluxes (i.e., the contribution of one axis of variability compared with the contribution of the other axes) is depicted in Figure 8. It shows the

**Figure 9.** (opposite) (a) Annual CO<sub>2</sub> concentration (ppm) simulated by TM2, TM3, and GCTM at all 46 stations with the a priori sources and sinks as defined before the inverse optimization, along with the observed concentrations. Stations are ordered by increasing latitude. (b) Contribution of the fossil fuel emissions only to the annual total concentration in Figure 9a. (c) Contribution of the annually balanced land biosphere only to the annual total concentration in Figure 9a. See color version of this figure at back of this issue.

percentage of the total external variance explained by the three axes of variability. For each parameter along one axis (e.g., TM2, TM3, and GCTM for the transport axis) we compute the average flux from the nine inversions that use this parameter (e.g., 3 time resolutions  $\times$  3 spatial resolutions in the foregoing example). We then take the variance of the three mean fluxes corresponding to one axis and report it as a fraction of the total variance (contribution in %). Note that the total contribution does not equal 100% because the inversions are not independent from each other. However, this simple diagnostic clearly shows that for Eurasia, transport uncertainty is the dominant factor (as noted in section 4.1) owing to the rectification gradients. On the other hand, transport is a less influential parameter for North America (where the time resolution was more important), at least for the stations and the regional breakdown that we used.

[47] Overall, there is a clear need to improve model transport characteristics when applying inversions at continental to regional scales. The recent TransCom 3 study, using many models [Gurney *et al.*, 2002] and a TIA approach, has investigated the sensitivity of the flux estimates to the transport model in detail and has emphasized the importance of understanding transport differences in the northern and tropical land regions.

#### 4.2. Time Resolution

[48] While model-dependent differences are responsible for some of the variability in the estimates, especially in terms of the latitudinal partitioning of the fluxes and the uptake in Eurasia, the time discretization method used (TIA for annual fluxes/annual data, TIm for annual fluxes/monthly data, and TDm for monthly fluxes/monthly data) also contributes a large part of the variability.

[49] Figure 8 shows that for North America and the North Atlantic, the two regions with the highest external covariance (see Table 7), almost all the variance can be attributed to differences among the time discretization methods. Much of this method-dependent variability can actually be explained by an anticorrelation between the estimates for North America and for the North Atlantic in just four of the experiments: those for the TIm method in the 12 and 17 region cases with the TM2 and TM3 models, as discussed in section 3.4.2. Figure 7 shows that in these cases an especially large uptake in North America of  $\sim -2.0$  GtC yr<sup>-1</sup> is counterbalanced by an out-gassing in the North Atlantic of  $\sim +0.5$  GtC yr<sup>-1</sup>. In the remaining cases these two adjacent regions take up  $-0.6$  and  $-0.9$  GtC yr<sup>-1</sup>, respectively, on average, with surprisingly good agreement among the different time resolutions. The external error for North America computed without the four TIm outliers is only 0.47 GtC yr<sup>-1</sup>, as compared with 0.65 GtC yr<sup>-1</sup> with them, and is only 0.32 for the North Atlantic, as compared with 0.58 GtC yr<sup>-1</sup> with them.

[50] One might expect beforehand that the annual adjustment/monthly data (TIm) method would be the most robust of all the time discretization methods, since it uses more measurements per flux solved for, and the information contained in the seasonal cycle of the measurements should provide an extra constraint not available in the TIA method. Apparently, though, this is not the case. Errors in the magnitude or phase of the a priori seasonal cycles of flux

can cause very large differences at the measurement sites in certain months. Matching the modeled concentrations with the observed ones for these few months drives the solution in quite a different direction than an inversion using annual mean measurements (TIA) would obtain. The TIm method thus might fit the seasonal cycle of the fluxes much more accurately than the TIA method, but it might do worse on the annual mean fluxes (see the discussion of the  $\chi^2$  statistic in section 5.1).

[51] Whatever is responsible for the outlying TIm results (i.e., those four cases with the out-gassing in the North Atlantic, Figure 7), it is surprising how similar the annual adjustment/annual data (TIA) and monthly adjustment/monthly data (TDm) cases are in terms of the annual mean fluxes. This gives us some confidence that the monthly flux inversion, even with its greater complexity, is rather robust. Our results argue against using the annual flux adjustment inversion using monthly data (TIm), however, a time resolution that has been widely used in previous studies [Rayner *et al.*, 1996; Bousquet *et al.*, 1999a; Taguchi, 1999; Ciais *et al.*, 1998].

#### 4.3. Spatial Resolution

[52] Another source of variability in the estimated fluxes arises from the use of large regions in the inversions. The relative spatial pattern of flux is fixed inside these regions, and since it is generally fixed to patterns that may disagree with the true ones, this can lead to biases in the estimated flux magnitudes. Kaminski *et al.* [2001] formally addressed this source of error (referring to it as “aggregation error”) and suggested solving for as many regions as computationally feasible to reduce it, then grouping them together afterward. However, when solving at high resolution (the highest resolution being the one of the transport model), no correlation are usually assumed between the errors on the a priori fluxes. One region can thus move away from its a priori value independently of the others. There is no a priori link in terms of CO<sub>2</sub> fluxes between them. We might thus argue that part of our knowledge of biogeochemical processes, as well as of the spatial patterns of the driving factors (i.e., climatic variables, fertilization by nitrogen deposition) is not taken into account in such approach. On the other hand, defining large spatially coherent regions is a way to set perfect correlations between different pixels grouped in a region. If only one part of the region is “seen” by the atmospheric network and further adjusted, the other unconstrained part will be adjusted in a similar way according to the a priori fluxes. In this case, such tight a priori correlations strongly influence the inverse solution.

[53] In this study, we performed inversions using three different spatial resolutions (3/4, 6/6, and 7/10 land/ocean regions, see Figure 2) to assess these errors to some extent. The use of two different models for the a priori flux patterns (the SiB2 model for the inversions using the TM2 and TM3 transport models and the CASA model for the inversions using GCTM) also helps to quantify this source of uncertainty.

[54] While the spatial resolution of the solved-for fluxes seems to cause less variability in the results than is contributed by the transport model and time discretization method, it does have an effect. Figure 8 shows that for the tropical land, a region with high variability across the

27-member sample ( $\sim 0.4 \text{ GtC yr}^{-1}$ ), almost all the variability is due to differences between the number of regions solved for. The results for the northern regions shift systematically as the resolution is increased from the 7-region case to the 12- and 17-region cases (see Table 4).

[55] The 12-region inversion has 7 regions in the extratropical north versus only 4 in the 7-region case. It should not be surprising, then, that the largest flux differences between these cases occurs in the north. In all the cases, except the TIm methods with TM2 or TM3 mentioned in section 3.4 (outlying cases), there is a tendency for uptake in North America to decrease and for uptake in Eurasia to increase when going from the 7- to the 12-region cases. In most of the cases the North Atlantic and Pacific do not change much, though there is a shift toward greater uptake in the North Atlantic in the 12-region T1a cases with TM2 or TM3. The lower North American uptake in the 12-region cases is due to out-gassing in the boreal part of the continent partially canceling out uptake in the temperate part when the North American continent is split into two regions (boreal and temperate). No such cancelation occurs within Eurasia. The 17-region inversion has 10 regions in the tropics and south versus only 5 in the 12-region case, so most of the differences in flux between the corresponding cases occur there. In the GCTM and TM3 cases the tropical oceans tend to have less out-gassing when they are subdivided, with the tropical land regions taking up less carbon to compensate. Most of the spread on the results for the tropics is thus related to the spatial resolution solved for. Finally, there is a tendency towards less uptake in the southern oceans in the TDm cases, especially when solving for 17 regions.

[56] It is quite possible that the shifts we see between the 7- and 12-region solutions are largely due to the removal of biases caused by assuming spatial patterns across the whole of Eurasia, North America, and the North Atlantic in the 7-region case. On the other hand, there may be other systematic errors that occur when solving for many regions. For example, the north-south flux difference for the 17-region GCTM monthly data/monthly flux case (TDm.gctm.r17) is much higher ( $-3.5 \text{ GtC yr}^{-1}$ ) than those for the other cases ( $-2.5 \text{ GtC yr}^{-1}$  for 7 regions and  $-2.7 \text{ GtC yr}^{-1}$  for 12 regions with this model, from Table 4). This is due to anticorrelations between the ill-constrained tropical land regions and the southern oceans: An anomalous out-gassing in the southern oceans is balanced by a large uptake in the southern part of the tropical land regions during the Southern Hemisphere summer. This large summer uptake in the southern part of South America and Africa is balanced by increased out-gassing during the rest of the year in those same land regions, resulting in relatively low annual mean uptakes for the whole of each region. The TDm inversion is thus using the time degree of freedom to create a north-south gradient within South America and Africa to help balance the overall north-south gradient of CO<sub>2</sub> in the atmosphere. While it is possible that this is what is occurring in the real world, it is more likely that this solution is a model artifact and that the inversion is placing anomalously large fluxes in poorly observed regions/months to force a better fit to the data. Thus one must also be careful to solve for the fluxes at a spatial resolution that can be adequately observed by the number of stations available. The example

above shows that systematic errors, as well as the random ones, will increase in this case.

[57] Overall, the optimal spatial resolution to solve for must minimize the sum of both the systematic and random errors. Such a choice is closely related to the information or model that we use to define the spatial patterns for the fluxes. What spatial patterns the land sink is assumed to have (distributed according to biome productivity (NPP), nitrogen fertilization, land use change, or other factors or a combination of these factors) is probably as important as using one particular model or one particular inverse scheme [Bousquet *et al.*, 1999b; Kaminski *et al.*, 2001]. Note that the TRANSCOM 3 inverse experiment [Gurney *et al.*, 2002] considers only one scenario for the spatial distribution of the fluxes (uniform over the oceans and using CASA net primary production for the land) together with spatially large regions. There is thus a need for a careful investigation of this source of uncertainty. This could be done by applying several flux models (biospheric and oceanic) to an atmospheric transport model. Some insights on this issue have already been provided by Heimann *et al.* [1998].

## 5. Consistency Check for the Inversions: Importance of A Priori Errors

[58] In this section, we examine a few diagnostics to assess the robustness of the results of the overall inverse procedure. We discuss the validity of the main underlying hypothesis of random Gaussian errors used in the synthesis inversion framework and also how we ensure a consistent statistical comparison between the inversions of the three time discretization methods (T1a, TIm, and TDm). We will also discuss the impact of the errors assumed for both the data and the a priori fluxes on the estimate.

### 5.1. Consistency of the Inversions: The $\chi^2$ Diagnostic

[59] As a first check of the realism of an inversion, one should examine the measurement residuals: the difference between the optimized concentrations and the observations. The standard deviation of these residuals should be, on average, proportional to the assumed measurement errors, and the residuals should be distributed as a Gaussian around the observed values. We have plotted the histograms of the residuals for our 27 inversions. Their distribution appears to be roughly symmetric, with rather short tails, and centered around zero, indicating no systematic bias in the modeled concentrations.

[60] As a second useful check, the consistency of the estimate with the measurement errors and the a priori flux errors assumed is analyzed using the global  $\chi^2$  statistic. The global  $\chi^2$  is defined as twice the cost function  $J(x)$  (equation (1)) at its minimum [see Tarantola, 1987, p. 212]:

$$\chi^2 = \sum_{i=0}^{N_{\text{obs}}} (y_i^a - y_i^o)^2 / R_i^o + \sum_{j=0}^{N_{\text{flux}}} (x_j - x_j^b)^2 / P_j^b. \quad (4)$$

The  $\chi^2$  value follows the so-called chi-square probability density, with the number of observations ( $N_{\text{obs}}$ ) as the number of degrees of freedom (because in our case the rank of the matrix is equal to the number of fluxes solved for). This  $\chi^2$  value, divided by  $N_{\text{obs}}$  (normalized  $\chi^2$ ), should

therefore be close to 1. A value  $>1$  indicates that the residuals (from the measurements and/or from the a priori fluxes) are larger than the uncertainties initially assumed. Deviations from 1.0 become statistically significant at the 95% confidence level outside the range  $1.0 \pm 0.4$  (assuming a  $\chi^2$  statistic with  $N_{obs} = 46$  degrees of freedom). Deviations larger than 1.4 should be avoided, as they indicate the violation of some hypothesis; for example, the errors for the measurements or the a priori sources might have been too small, or the response functions calculated with the transport model are too far from reality, or both. On the other hand, a  $\chi^2$  lower than 1 indicates that we could have decreased the initial data errors to ensure a better fit between model and data.

[61] Table 5 shows the values for normalized  $\chi^2$  for each model and time resolutions, averaged across the different spatial resolutions (since they give similar values). First of all, we notice that except for the annual adjustment/annual data inversions (T1a), the  $\chi^2$  for all three models are lower than or close to 1, which indicates that we were consistent in the way we set the initial uncertainties. The  $\chi^2$  values are significantly lower in the case of monthly fluxes (TDm) than in the case of annual fluxes (T1m). This difference reflects a better fit to seasonal data when the sources are adjusted on a monthly basis (TDm) compared with the case where only their annual magnitude is adjusted (fixed seasonality in T1m). For the annual adjustment/annual data inversions (T1a) the  $\chi^2$  values are above the level of significance for all transport models (1.4 for 46 degrees of freedom). The relative contribution of the measurement term to the total  $\chi^2$  (equation (4) or cost function at its minimum) is much larger than that of the flux term (88% versus 12% on average), indicating that the a priori constraints are fairly loose.

[62] Thus for the T1a inversions the uncertainties on the annual mean data are the ones that are probably too low. Recall that we used the hypothesis of independence between monthly errors to compute the annual errors (equation (2)) in order to statistically compare the different time discretization methods (T1a, T1m, and TDm). Such an assumption leads to relatively low annual errors (monthly errors divided by  $\sqrt{12}$ ), which seem to be incompatible with the annual response function. This diagnostic suggests that we should reconsider the hypothesis of independent monthly errors for each station when computing annual errors for the T1a method. In order to get  $\chi^2$  in the T1a cases that are similar to those in the T1m cases (i.e., closer to 1), we estimate that the monthly error should be divided by the square root of 4 instead of 12. This would mean that the measurement errors are highly correlated on average over 3 consecutive months, leading effectively to only four independent measurements (instead of 12). The implication of this in terms of the flux estimates has not been examined yet. The best way to treat correlations between the individual monthly data error would be to solve the inverse problem with some non-diagonal a priori covariance matrix to account for the correlations. We nevertheless believe that the impact will be limited, although such analysis is currently under investigation.

[63] Note that the  $\chi^2$  values for the inversions in which all ocean fluxes were fixed to their a priori value of Takahashi *et al.* [1999] (the “fixed at 2.0 GtC yr<sup>-1</sup>” case

in Figure 5) are always larger than the  $\chi^2$  values for the inversion, in which the ocean fluxes are solved for regionally. As noted in section 3, this indirectly confirms the fact that within our inverse setup, the atmospheric data do not support a large ocean sink, especially in the south.

## 5.2. Relative Weight Between Stations: Influence of Particular Sites

[64] In addition to the global consistency between data errors and a priori flux errors one should also assess the validity of the relative weights (inverse of the squared data error) assumed for the individual measurement residuals (i.e., at each station). These weights are crucial for partitioning the CO<sub>2</sub> sources and sinks spatially. In this study, we calculated monthly measurement errors from the root mean square of the residuals between the raw data and a seasonal fitted curve (see section 2.3). For certain stations, only a few measurements are available, which may yield an unrealistically low estimate of the error. The inverse solution might then be biased by these few sites, especially if the a priori modeled concentrations do not match the data well (i.e., are not within 1 $\sigma$  error). In order to check for such outlier stations, we display in Figure 11 the individual contribution of each site to the cost function  $J(x)$  (equation (1)) for the 7-region cases ( $(y_i^a - y_i^o)^2/R_i^o$ ). This quantity can be also described as a “ $\chi^2$  per station,” as it represents the contribution of each site to the first term (the dominant term) of the global  $\chi^2$  (equation (4)). For monthly data inversions (T1m and TDm) the 12 monthly contributions are summed in Figure 11.

[65] As a general feature, the relative influence of each site to the solution significantly differs between the three models. Moreover, a few stations appear to contribute more than others to the cost function  $J(x)$ . For the annual adjustment/annual data inversions (T1a) we notice large values (above 10) for few stations in the Southern Hemisphere (CO2, P14, CGO, CRZ) compared with the northern sites which are mostly below 5 (except three sites in the north for the GCTM model). Note that a value from 9 to 25 indicates that the model concentration differs from the observed one by 3 to 5 times the data error. For the annual adjustment/monthly data (T1m) inversions the contributions of QPC and RPB to  $J(x)$  appear clearly as outliers for the TM3 model. In the case of QPC it is linked to a large mismatch during the summer months. For the monthly adjustment/monthly data (TDm) inversions we do not observe the same problem at QPC that we did with T1m (using TM3) because the inversion is now able to correct summer fluxes independently from winter ones.

[66] In general, the presence of a few stations with much larger contributions to  $J(x)$  than the other stations means that the a priori errors for these particular sites were chosen too low. It is thus important to verify that they do not completely drive the inverse solution. If so, one should carefully investigate the pertinence of such a choice. As a sensitivity test, we removed stations QPC and RPB from the T1m inversion with TM3. The estimated CO<sub>2</sub> uptake increases by 0.3 GtC yr<sup>-1</sup> over Eurasia compared with the control case, while decreasing by the same amount in the tropics. Such changes, although not drastic, point to the importance of the choice of the individual station data errors. For inversions with annual data (the T1a cases) the Southern

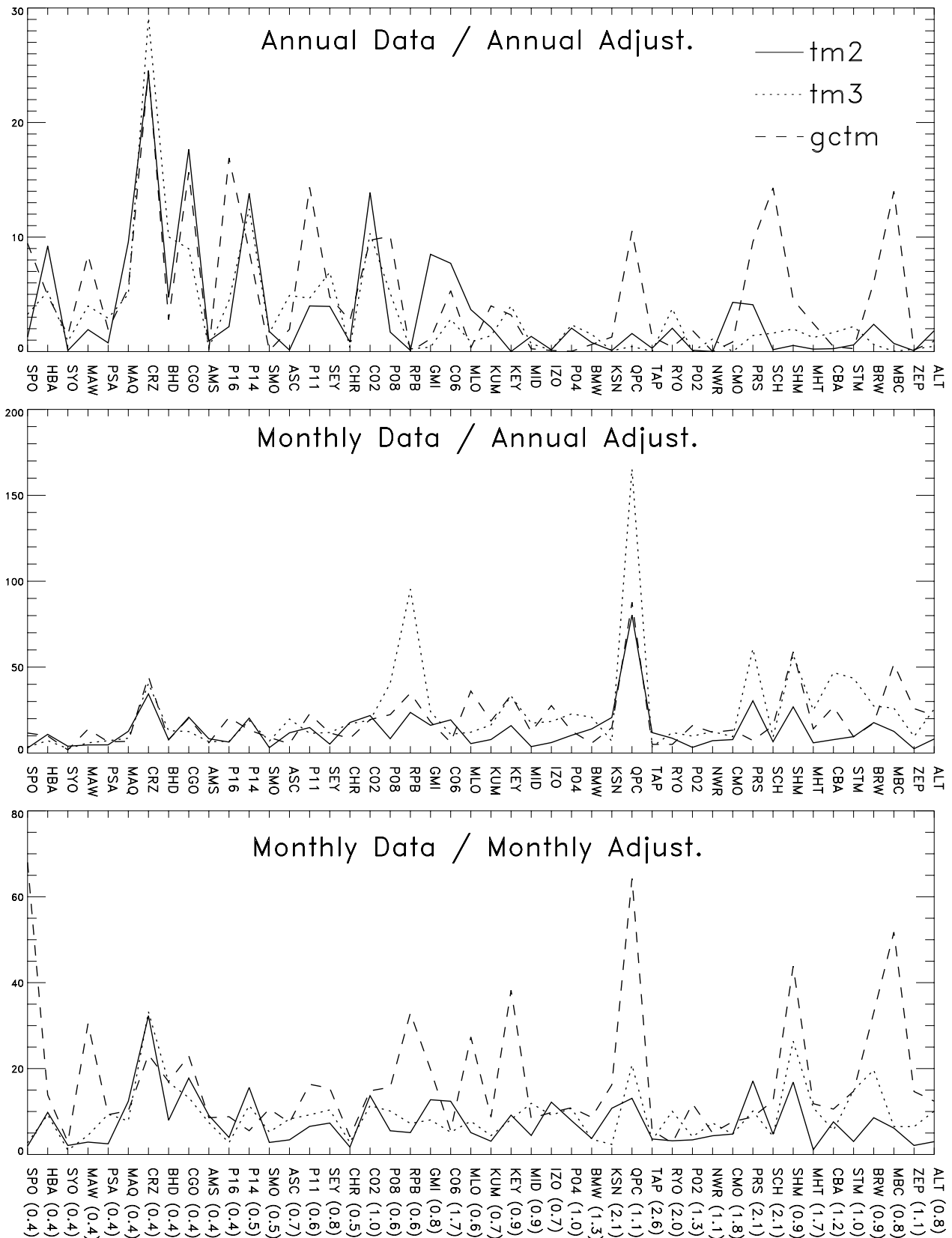


**Figure 11.** Contributions of each station to the misfit function  $J(x)$  (equation (1)) at its minimum (or the global  $\chi^2$ ) for the 7-regions inversions: 3 models  $\times$  3 time-resolution methods (three graphs). These contributions are the terms of the first right member in equation (4), section 5.1. For monthly data inversions the 12 monthly contributions are summed for each station. Stations are ordered by decreasing latitude from north to south, and the numbers in parenthesis represent the monthly data a priori uncertainties.

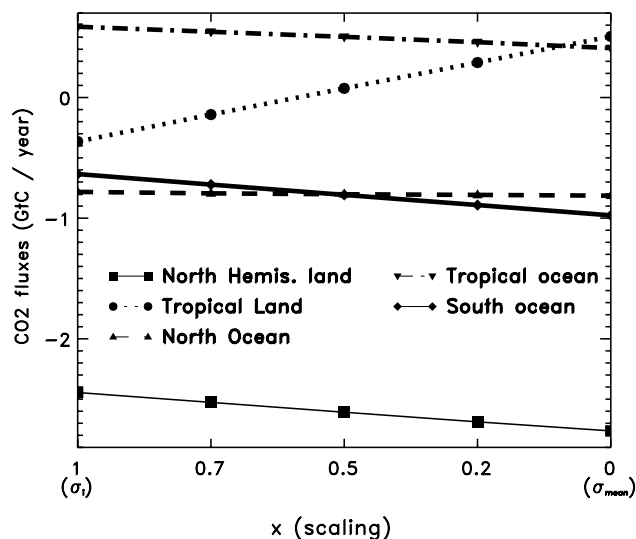
Hemisphere sites have fairly small annual errors compared with the northern sites,  $\sim 0.13$  ppm versus  $\sim 0.50$  ppm, respectively. These errors are simply the monthly ones (number in parentheses, Figure 11c) divided by  $\sqrt{12}$ . This is why the contribution of the Southern Hemisphere sites to the inverse solution is enlarged (Figure 11a).

[67] For the data errors, most of inverse studies published so far use either a constant value for all sites [Rayner *et al.*, 1999; Fan *et al.*, 1998; Enting *et al.*, 1995] or an approach similar to ours (see section 2.2) [Bousquet *et al.*, 1999a; Peylin *et al.*, 1999; Kaminski *et al.*, 1999; Baker, 2001]. We performed a sensitivity test where we progressively smoothed all data errors ( $\sigma_i$ ) to the limiting case where all sites have the same mean monthly data error,  $\sigma_{\text{mean}} = 0.92$  ppm, according to  $\sigma_{\text{new}} = \sigma_{\text{mean}} * (\sigma_i/\sigma_{\text{mean}})^x$  with  $x = 0$  to 1. Leveling the errors ( $x = 0$ ) enhances the weight of the Northern Hemisphere sites in the inversion and decreases the weight of the Southern Hemisphere sites compared with our standard case ( $x = 1$ ). Figure 12 presents annual mean CO<sub>2</sub> fluxes aggregated over large regions and averaged across all 27 inversions for five different sets of data errors. In the “constant error” case ( $x = 0$ ,  $\sigma = \sigma_{\text{mean}}$ ) the southern ocean sink and the Northern Hemisphere land sink are increased by  $\sim 0.3$  GtC yr<sup>-1</sup> each compared with the standard case, while the tropical land compensates to maintain the global CO<sub>2</sub> budget ( $+0.8$  GtC yr<sup>-1</sup>). The inverse solution, although not drastically changed, is thus fairly sensitive to the relative weight between stations. This is even more crucial when one considers a finer regional breakdown (e.g., R17 regions). Note also that Figure 12 only displays an average of the 27 flux estimates, which strongly smoothes the flux variations.

[68] Overall, the choice of data errors for an inversion requires great care. It has to satisfy not only global consistency between a priori data errors and flux errors (see section 3.4.1) but also must ensure that a few particular sites do not nudge the inverse solution excessively. We have discussed here important diagnostics to consider in order to control these potential pitfalls. Recall that in the framework of Bayesian synthesis inversions, described by the cost function  $J(x)$  (equation (1)), the data error matrix  $R^o$  should contain the observational uncertainty as well as the uncertainties due to model error [Tarantola, 1987]. More precisely, it should comprise instrumental error; intercalibration error between networks (if needed); sampling error, both in space and time, including those due to the selection criteria of air masses at most stations; intrinsic error of the transport model; aggregation error due to the fact that we assume spatial patterns for the sources inside of large regions [Kaminski *et al.*, 2001]; and the use of the wrong wind fields for the span considered. In principle, we should try to quantify all these terms. The use in  $R^o$  of the standard deviation of the residuals between raw data and a cyclical function (this approach is used in most of the inverse studies published so far) is oversimplified and rather inaccurate.

### 5.3. Interdependence on the A Priori Flux Errors

[69] The choice of constraining the fluxes to some a priori estimate to within its given uncertainty (second term in the cost function  $J(x)$ ) allows an optimal use of available information and is an essential part of stabilizing the ill-conditioned tracer inversions in the Bayesian approach. In



$$\text{Data error : } \sigma_{\text{new}} = \sigma_{\text{mean}} * (\sigma_i/\sigma_{\text{mean}})^x$$

**Figure 12.** Annual CO<sub>2</sub> fluxes in GtC yr<sup>-1</sup> as function of the data uncertainties and reported for five regions (aggregated from the seven regions breakdown). Differences between data uncertainties as defined from the GLOBALVIEW database are progressively smoothed according to  $\sigma_{\text{new}} = \sigma_{\text{mean}} * (\sigma_i/\sigma_{\text{mean}})^x$ , with  $x$  taking the values 1 (standard case,  $\sigma_i$ ), 0.7, 0.5, 0.2, and 0.0 (limit case of a constant uncertainty for all site defined as the mean standard uncertainties,  $\sigma_{\text{mean}} = \sum_{i=1}^{N_{\text{obs}}} \sigma_i$ ).

this respect the values of the a priori flux errors need to be chosen carefully. Small a priori errors correspond to the perspective that the corresponding fluxes are already well known; in that case atmospheric data are less likely to improve our a priori knowledge on the fluxes. On the other hand, errors correspond to the perspective of a “blind inversion” where atmospheric data are the main source of information. In this study, we specified fairly large errors for the air-sea flux (1 GtC yr<sup>-1</sup> per basin) and even larger error for the net land uptake (2 GtC yr<sup>-1</sup> per region), except for the tropical land regions (1 GtC yr<sup>-1</sup>, to avoid some large dipoles between these poorly constraint regions). Note that for the gross biospheric fluxes that we solve for (GPP and RES of SiB2 for TM2 and TM3 and NPP and RES<sub>h</sub> of CASA for GCTM), we set very large errors (50% of the flux). Such a choice is somewhat arbitrary and favors information from atmospheric data.

[70] We performed sensitivity tests in which we varied the a priori errors on the net fluxes, ranging from very tight errors to very loose ones, as in Bousquet *et al.* [1999b]. Large changes in the estimated fluxes ( $>0.5$  GtC yr<sup>-1</sup> per region) appear when the flux errors are decreased by more than a factor of 2 as compared with the standard case. On the other hand, only slight changes appear when the errors are loosened (at least in the 7-region cases; in the 17-region cases changes up to 0.3 GtC yr<sup>-1</sup> occur in the optimized fluxes). Such results indicate that the standard inversion lies in the range where the solution only slightly depends on the a priori errors, at least for small numbers of regions (7-region and 12-region cases). Solving for a larger number

**Table 8.** Mean Inversion Results Across the Whole 27-Experiment Sample (All) and Without the Annual Adjustment/Monthly Data Method (No TIm), in the 7 Regions Breakdown<sup>a</sup>

Case	NH Land	NH Oce	Trop. Land	Trop. Oce.	South. Oce.
All	-2.45 ± .34/.77	-0.78 ± .28/.61	-0.36 ± .39/.38	0.59 ± .19/.27	-0.63 ± .15/.25
No TIm	-2.16 ± .40/.55	-1.05 ± .33/.41	-0.41 ± .42/.27	0.56 ± .20/.27	-0.58 ± .16/.29
Case	NH Total	N. Amer.	Eurasia	N. Paci.	N. Atlan.
All	-3.23 ± 17/0.31	-0.79 ± .43/.65	-1.66 ± .38/.57	-0.12 ± .17/.21	-0.66 ± .26/.58
No TIm	-3.21 ± .19/.25	-0.52 ± .49/.47	-1.64 ± .44/.59	-0.13 ± .19/.25	-0.92 ± .29/.31

<sup>a</sup>The “mean internal” and the “external” errors are added (in GtC yr<sup>-1</sup>).

of regions than used in this study would require greater care in defining error on the a priori fluxes.

## 6. Summary and Conclusions

[71] We have carried out a series of synthesis inversions to investigate the robustness of current inverse approaches and also to identify the components of the inversion that are most responsible for the scatter obtained in the regional fluxes published to date (Table 1). The inversions were performed using data from 46 atmospheric measurement sites [*GLOBALVIEW-CO<sub>2</sub>*, 1999] with Bayesian a priori values to regularize the solution [*Tarantola*, 1987]. To assess the sensitivity, we systematically varied one parameter or component of the inversion after another: the atmospheric transport (TM2, TM3, and GCTM models), time discretization of the data and the fluxes (monthly or annual), spatial resolution of the fluxes (7, 12, and 17 regions), and the tightness of a constraint on the global ocean flux total. These axes of variability are summarized in Figure 3. The main results of this study can be divided into biogeochemical implications for the regional carbon balance and suggestions for further improvement of inverse studies.

### 6.1. Biogeochemical Results

[72] The results of our 27 inversions (3 models × 3 time discretization × 3 spatial discretization) using a global ocean uptake constraint of  $-2.0 \pm 0.8$  GtC yr<sup>-1</sup> show that the flux estimates appear to be robust (i.e., with little scatter) when considering total flux (land plus ocean) over large zonal areas. For the 1990–1994 period we estimate a large CO<sub>2</sub> sink north of 30°N ( $-3.2 \pm 0.3$  GtC yr<sup>-1</sup>), a small source over the tropical band ( $+0.2 \pm 0.35$  GtC yr<sup>-1</sup>), and a surprisingly small sink south of 30°S ( $\sim -0.6 \pm 0.25$  GtC yr<sup>-1</sup>). Recall that the global uptake for this period was quite large compared with the average for the 1980s and 1990s; our set of inversions tends to locate this enhanced sink mainly at high northern latitudes, especially over land.

[73] The mean global ocean uptake of  $-0.9$  GtC yr<sup>-1</sup> ( $-1.1$  GtC yr<sup>-1</sup> without the spurious TIm cases discussed in section 3) is smaller than the  $-2.2$  GtC yr<sup>-1</sup> estimate of *Takahashi et al.* [1999] and the estimates of independent studies using O<sub>2</sub>/N<sub>2</sub> atmospheric data [*Battle et al.*, 2000] or a suite of ocean carbon cycle models [*Orr et al.*, 2001] ( $-2.0$  and  $-2.2$  GtC yr<sup>-1</sup>, respectively). More precisely, the discrepancy between our ocean flux estimates and theirs occurs predominantly in the southern ocean, where the inversions tend to produce a much smaller sink (from  $-1.1$  to  $+0.1$  GtC yr<sup>-1</sup>). These low values primarily reflect the need to match the model north-south gradient to the

shallower observed one. Possible explanations for the gradient mismatch may be (1) interhemispheric mixing in the transport models that is too fast and (2) a “rectifier” over northern latitudes that is too strong, which would need to be compensated for by a large sink over these regions (and conversely a smaller sink in the southern ocean). The total uptake is well defined by the atmospheric global CO<sub>2</sub> growth rate. On the other hand, a large preindustrial source of CO<sub>2</sub> in the Southern Hemisphere (from river fluxes or ocean transport) might also bridge the gap. Further investigation is needed to resolve this important disagreement.

[74] When considering the longitudinal breakdown of the fluxes in the north (i.e., between North America, Eurasia, North Atlantic, and North Pacific or even simply between the land and ocean) the spread between all our estimates increases. This spread, referred to here as the “external uncertainty,” as opposed to the “internal uncertainty” given by the inverse procedure, is important to consider. The “external uncertainties,” which provide an estimate of the systematic errors, appear to be larger than the “internal uncertainties,” except for tropical land where the lack of measurement seems to be the most critical issue (Table 8). If the results of all 27 cases are considered, the spread is large enough to make it difficult to draw a clear picture of the regional carbon balance in the north. If we reject the suspicious TIm results, however, the spread for the North Atlantic drops to a level ( $0.3$  GtC yr<sup>-1</sup>) at which it seems fairly well constrained; the spreads for Eurasia and North America are then low enough to begin to believe their partitioning, as well. In either case, for 1990–1994 our ensemble of inversions tends to favor larger uptake over Eurasia than over North America and the North Atlantic ( $-1.6$ ,  $-0.5$ , and  $-0.9$  GtC yr<sup>-1</sup>, respectively, without the TIm cases), with a smaller uptake in the North Pacific.

### 6.2. Recommendations

[75] In this study, we have investigated some of the systematic errors that can arise from using a particular transport model, using an annual or monthly temporal discretization, and solving for different numbers of regions. Among these sources of errors, we found that (1) the choice of time resolution is crucial in partitioning the CO<sub>2</sub> sink between North America and North Atlantic, (2) the uncertainty on the transport dominates the “external uncertainty” for Eurasia, and (3) the spatial resolution (number of regions solved for) was the main factor only for the tropics (Figure 8). This analysis has shown the importance of the time resolution in the spread of the regional estimates, an aspect poorly documented until now. We found that using an annual adjustment with monthly data (TIm method) gave

the most unlikely results (with TM2 and TM3). This approach and maybe more generally an approach where one solves for fluxes at a finer time step than the time discretization of the data, can be highly sensitive to particular data (depending on the value of the response function, i.e.,  $H$  term in equation (1)). The TIm method thus appears to be less robust and needs to be used with great care. For the spatial resolution we believe that there is an optimal number of regions to solve for that minimizes the sum of the random estimation error and the systematic aggregation errors. A more detail analysis needs to be made to be sure, but the results from our sparse resolution case (seven regions) may show large biases in the estimated fluxes in the Northern Hemisphere. This “aggregation problem” is also directly linked to the choice of the a priori patterns for the fluxes within each region. Such choice should be further investigated, as different scenarios for the land uptake of carbon are highly debated.

[76] The choice of data errors also appears to be a critical step that requires great care. As a useful check, the consistency between data errors and a priori errors should at least be achieved with the global  $\chi^2$  diagnostic (its value should not be greater than one [Tarrantola, 1987]). Moreover, one should also check the distribution of the residuals (or the contribution of each station to the cost function) in order to verify that the inverse solution is not driven by only few specific sites. There is a crucial need to better define the data errors (in a physical sense) and to account for the correlations in time (and probably in space) between those errors. The choice of the a priori flux errors can be also important. We chose in this study to set large a priori errors for ocean fluxes, which might underestimate our current knowledge of ocean biogeochemistry, rather than risk the possibility of overconstraining the inversion.

[77] **Acknowledgments.** We thank P. Monfray for early discussions which helped direct this work. The Commissariat à l’Énergie Atomique and The Centre National d’Étude Spatiale (CNES) partly funded this work and contributed to the computing resources. We thank NASA’s Graduate Student Researchers Program (NASA Training Grant NGT5-61) for supporting DFB. NOAA’s Office of Global Programs and the Geophysical Fluid Dynamics Laboratory provided funding and computer time.

## References

- Andres, R. J., G. Marland, and S. Bischoff, Carbon dioxide emissions from fossil fuel combustion and cement manufacture 1751–1991 and an estimate of their isotopic composition and latitudinal distribution, in *1993 Global Change Institute*, edited by T. Wigley and D. Schimel, pp. 419–429, Cambridge Univ. Press, New York, 1996.
- Aumont, O., J. C. Orr, P. Monfray, W. Ludwig, P. Amiotte-Suchet, and J. L. Probst, Riverine-driven interhemispheric transport of carbon, *Global Biogeochem. Cycles*, *15*, 393–406, 1999.
- Baker, D., An inversion method for determining time-dependent surface CO<sub>2</sub> fluxes, in *Inverse Methods in Global Biogeochemical Cycles*, *Geophys. Monogr. Ser.*, vol. 114, edited by P. Kasibhatla et al., pp. 279–295, AGU, Washington, D. C., 1999.
- Baker, D., Sources and sinks of atmospheric CO<sub>2</sub> estimated from batch least-squares inversion of CO<sub>2</sub> concentration measurements, Ph.D. thesis, Princeton Univ., Princeton, N. J., 2001.
- Battle, M., M. L. Bender, P. P. Tans, J. W. C. White, J. T. Ellis, T. Conway, and R. J. Francey, Global carbon sinks and their variability inferred from atmospheric O<sub>2</sub> and  $\delta^{13}\text{C}$ , *Science*, *287*, 2467–2469, 2000.
- Battle, M., et al., Atmospheric gas concentrations over the past century measured in air from firm at the South Pole, *Nature*, *383*, 231–235, 1996.
- Bousquet, P., Optimisation des flux de CO<sub>2</sub>: assimilation des mesures atmosphériques en CO<sub>2</sub> et en  $^{13}\text{C}$  dans un modèle de transport tridimensionnel, Ph.D. thesis, Univ. Paris VI, Paris, 1997.
- Bousquet, P., P. Ciais, P. Peylin, and P. Monfray, Optimization of annual atmospheric CO<sub>2</sub> net sources and sinks using inverse modeling, 1, Method and control inversion, *J. Geophys. Res.*, *104*, 26,161–26,178, 1999a.
- Bousquet, P., P. Peylin, P. Ciais, M. Ramonet, and P. Monfray, Optimization of annual atmospheric CO<sub>2</sub> net sources and sinks using inverse modeling, 2, Sensitivity study, *J. Geophys. Res.*, *104*, 26,179–26,193, 1999b.
- Bousquet, P., P. Peylin, P. Ciais, P. Rayner, P. Friedlingstein, C. Lequere, and P. Tans, Interannual CO<sub>2</sub> sources and sinks as deduced by inversion of atmospheric CO<sub>2</sub> data, *Science*, *290*, 1342–1346, 2000.
- Ciais, P., et al., Partitioning of ocean and land uptake of CO<sub>2</sub> as inferred by  $\delta^{13}\text{C}$  measurements from the NOAA climate monitoring and diagnostics laboratory global air sampling network, *J. Geophys. Res.*, *100*, 5051–5070, 1995.
- Ciais, P., P. Peylin, and P. Bousquet, The regional distribution of the biospheric carbon fluxes as inferred from atmospheric CO<sub>2</sub> measurements and models, paper presented at Science Conference, Global Change and Terr. Ecosyst.-Land Use/Cover Change, Stanford, Calif., March 1998.
- Cramer, W., et al., Comparing global models of terrestrial net primary productivity (NPP): Overview and key results, *Global Change Biol.*, *5*(suppl. 1), 1–15, 1999.
- Denning, A., et al., Three-dimensional transport and concentration of SF<sub>6</sub>: A model intercomparison study (TransCom 2), *Tellus, Ser. B*, *51*, 266–297, 1999.
- Denning, A. S., I. Fung, and D. Randall, Latitudinal gradient of atmospheric CO<sub>2</sub> due to seasonal exchange with land biota, *Nature*, *376*, 240–243, 1995.
- Denning, A. S., G. J. Collatz, C. Zhang, D. A. Randall, J. A. Berry, P. J. Sellers, G. D. Colello, and D. A. Dazlich, Simulations of terrestrial carbon metabolism and atmospheric CO<sub>2</sub> in a general circulation model, 1, Surface carbon fluxes, *Tellus, Ser. B*, *48*, 521–542, 1996.
- Enting, I. G., Green’s function methods of tracer inversion, in *Inverse Methods in Global Biogeochemical Cycles*, *Geophys. Monogr. Ser.*, vol. 114, edited by P. Kasibhatla et al., pp. 19–32, AGU, Washington, D. C., 1999.
- Enting, I. G., C. M. Trudinger, R. J. Francey, and H. Granek, Synthesis inversion of atmospheric CO<sub>2</sub> using the GISS tracer transport model, *Tech. Rep. 29*, Commonw. Sci. and Ind. Res. Org. Div. Atmos. Res., Australia, 1993.
- Enting, I. G., C. M. Trudinger, and R. J. Francey, A synthesis inversion of the concentration and  $\delta^{13}\text{C}$  of atmospheric CO<sub>2</sub>, *Tellus, Ser. B*, *47*, 35–52, 1995.
- Fan, S., M. Gloor, J. Mahlman, S. Pacala, J. Sarmiento, T. Takahashi, and P. Tans, Atmospheric and oceanic CO<sub>2</sub> data and models imply a large terrestrial carbon sink in North America, *Science*, *282*, 442–446, 1998.
- GLOBALVIEW-CO<sub>2</sub>, Cooperative Atmospheric Data Integration Project—Carbon dioxide, Tech. rep. [CD-ROM], Natl. Ocean. Atmos. Admin./Clim. Monitor. Diagn. Lab., Boulder, Colo., 1999 (Available on internet via anonymous FTP at ftp.cmdl.noaa.gov, path: ccg/CO<sub>2</sub>/GLOBALVIEW).
- Gloor, M., S.-M. Fan, S. W. Pacala, and J. L. Sarmiento, Optimal sampling of the atmosphere for purpose of inverse modeling—A model study, *Global Biogeochem. Cycles*, *14*, 407–428, 2000.
- Gurney, K. R., et al., Towards robust regional estimates of annual mean CO<sub>2</sub> sources and sinks, *Nature*, *415*, 626–630, 2002.
- Heimann, M., et al., Evaluation of terrestrial carbon cycle models through simulations of the seasonal cycle of atmospheric CO<sub>2</sub>: First results of a model intercomparison study, *Global Biogeochem. Cycles*, *12*, 1–24, 1998.
- Hein, R., P. J. Crutzen, and M. Heimann, An inverse modeling approach to investigate the global atmospheric methane cycle, *Global Biogeochem. Cycles*, *11*, 43–76, 1997.
- Houghton, R. A., Interannual variability in the global carbon cycle, *J. Geophys. Res.*, *105*, 20,121–20,130, 2000.
- IPCC, *Radiative Forcing of Climate Change and an Evaluation of the IPCC IS92 Emission Scenarios*, Cambridge Univ. Press, New York, 1995.
- Kaminski, T., M. Heimann, and R. Giering, A coarse grid three dimensional global inverse model of the atmospheric transport, 2, Inversion of the transport of CO<sub>2</sub> in the 1980s, *J. Geophys. Res.*, *104*, 18,555–18,581, 1999.
- Kaminski, T., P. J. Rayner, M. Heimann, and I. G. Enting, On aggregation errors in atmospheric transport inversions, *J. Geophys. Res.*, *106*, 4703–4715, 2001.
- Keeling, C. D., S. C. Piper, and M. Heimann, A three-dimensional model of atmospheric CO<sub>2</sub> transport based on observed winds, 4, Mean annual gradients and interannual variations, in *Aspects of Climate Variability in the Pacific and the Western Americas*, *Geophys. Monogr. Ser.*, vol. 55, edited by P. D. H., pp. 305–363, AGU, Washington, D. C., 1989.
- Keeling, R. F., S. C. Piper, and M. Heimann, Global and hemispheric CO<sub>2</sub> sinks deduced from changes in atmospheric O<sub>2</sub> concentration, *Nature*, *381*, 218–221, 1996.

- Kicklighter, D. W., et al., A first-order analysis of the potential role of CO<sub>2</sub> fertilization to affect the global carbon budget: A comparison of four terrestrial biosphere models, *Tellus, Ser. B*, 51, 343–366, 1999.
- Langenfelds, R. L., R. J. Francey, L. P. Steele, M. Battle, R. F. Keeling, and W. F. Budd, Partitioning of the global fossil CO<sub>2</sub> sink using a 19-year trend in atmospheric O<sub>2</sub>, *Geophys. Res. Lett.*, 26, 1897–1900, 1999.
- Law, R. M., and P. J. Rayner, Impacts of seasonal covariance on CO<sub>2</sub> inversions, *Global Biogeochem. Cycles*, 13, 845–856, 1999.
- Law, R. M., et al., Variations in modeled atmospheric transport of carbon dioxide and the consequences for CO<sub>2</sub> inversions, *Global Biogeochem. Cycles*, 10, 783–796, 1996.
- Masarie, K. A., and P. Tans, Extension and integration of atmospheric carbon dioxide data into a globally consistent measurement record, *J. Geophys. Res.*, 100, 11,593–11,610, 1995.
- Orr, J. C., et al., Estimates of anthropogenic carbon uptake from four three-dimensional global ocean models, *Global Biogeochem. Cycles*, 15, 43–60, 2001.
- Peylin, P., P. Bousquet, P. Ciais, and P. Monfray, Differences of CO<sub>2</sub> flux estimates based on a time-independent versus a time-dependent inversion method, in *Inverse Methods in Global Biogeochemical Cycles*, *Geophys. Monogr. Ser.*, vol. 114, edited by P. Kasibhatla et al., pp. 295–309, AGU, Washington, D. C., 1999.
- Potter, C. S., J. T. Randerson, C. B. Field, P. A. Matson, P. M. Vitousek, H. A. Mooney, and S. A. Klooster, Terrestrial ecosystem production: A process model based on global satellite and surface data, *Global Biogeochem. Cycles*, 7, 811–841, 1993.
- Rayner, P., I. Enting, and C. Trudinger, Optimising the CO<sub>2</sub> observing network for constraining sources and sinks, *Tellus, Ser. B*, 48, 433–444, 1996.
- Rayner, P., I. Enting, R. Francey, and R. Langenfelds, Reconstructing the recent carbon cycle from atmospheric CO<sub>2</sub>, δ<sup>13</sup>C and O<sub>2</sub>/N<sub>2</sub> observations, *Tellus, Ser. B*, 51, 213–232, 1999.
- Sarmiento, J. L., and E. T. Sundquist, Revised budget for the oceanic uptake of anthropogenic carbon dioxide, *Nature*, 356, 593–598, 1992.
- Sarmiento, J. L., P. Monfray, E. Maier-Reimer, O. Aumont, and J. Orr, Sea-air fluxes and carbon transport: A comparison of three ocean general circulation models, *Global Biogeochem. Cycles*, 14, 1267–1281, 2000.
- Sellers, P. J., D. R. Randall, G. J. Collatz, J. A. Berry, C. B. Field, D. A. Dazlich, C. Zhang, G. D. Collelo, and L. Bounoua, A revised land surface parameterization (SiB2) for atmospheric GCMs, I, Model formulation, *J. Clim.*, 9, 676–705, 1996.
- Taguchi, S., Synthesis inversion of atmospheric CO<sub>2</sub> using the NIRE chemical transport model, in *Inverse Methods in Global Biogeochemical Cycles*, *Geophys. Monogr. Ser.*, vol. 114, edited by P. Kasibhatla et al., pp. 239–254, AGU, Washington, D. C., 1999.
- Takahashi, T., R. A. Feely, R. Weiss, R. H. Wanninkhof, D. W. Chipman, S. C. Sutherland, and T. T. Takahashi, Global air-sea flux of CO<sub>2</sub>: An estimate based on measurements of sea-air P<sub>CO<sub>2</sub></sub> difference, in *Proceedings of the National Academy of Science*, vol. 94, p. 8929, Natl. Acad. of Sci., Washington, D. C., 1997.
- Takahashi, T., R. H. Wanninkhof, R. A. Feely, R. F. Weiss, D. W. Chipman, N. Bates, J. Olafsson, C. Sabine, and S. C. Sutherland, Net sea-air CO<sub>2</sub> flux over the global oceans: An improved estimate based on the sea-air pCO<sub>2</sub> difference, paper presented at 2nd International Symposium of CO<sub>2</sub> in the Oceans, Center for Global and Env. Res., Tsukuba, Japan, 1999.
- Tans, P. P., I. Y. Fung, and T. Takahashi, Observational constraints on the global atmospheric CO<sub>2</sub> budget, *Science*, 247, 1431–1438, 1990.
- Tarantola, A., *Inverse Problem Theory*, Elsevier Sci., New York, 1987.
- Thoning, K. W., P. P. Tans, and W. D. Komhyr, Atmospheric carbon dioxide at Mauna Loa Observatory, 2, Analysis of the NOAA GMCC data, 1974–1985, *J. Geophys. Res.*, 94, 8549–8565, 1994.
- Wanninkhof, R., Relationship between wind speed and gas exchange over the ocean, *J. Geophys. Res.*, 97, 7373–7382, 1992.

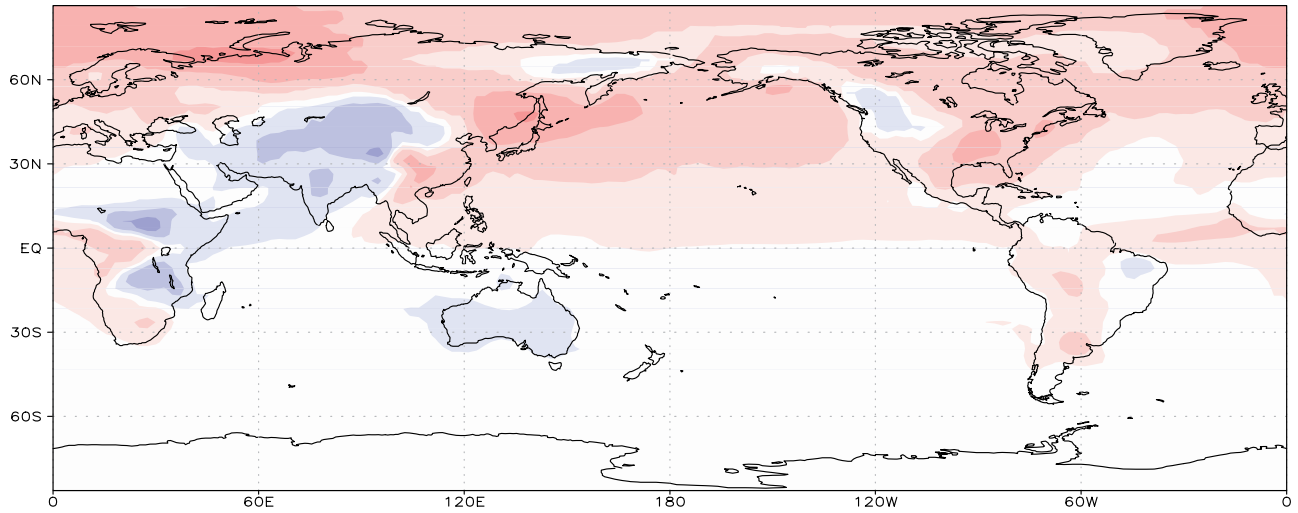
---

D. Baker and J. Sarmiento, Atmospheric and Oceanic Sciences Program, Princeton University, Princeton, NJ 08544-0710, USA. (dfb@cgd.ucar.edu; jls@princeton.edu)

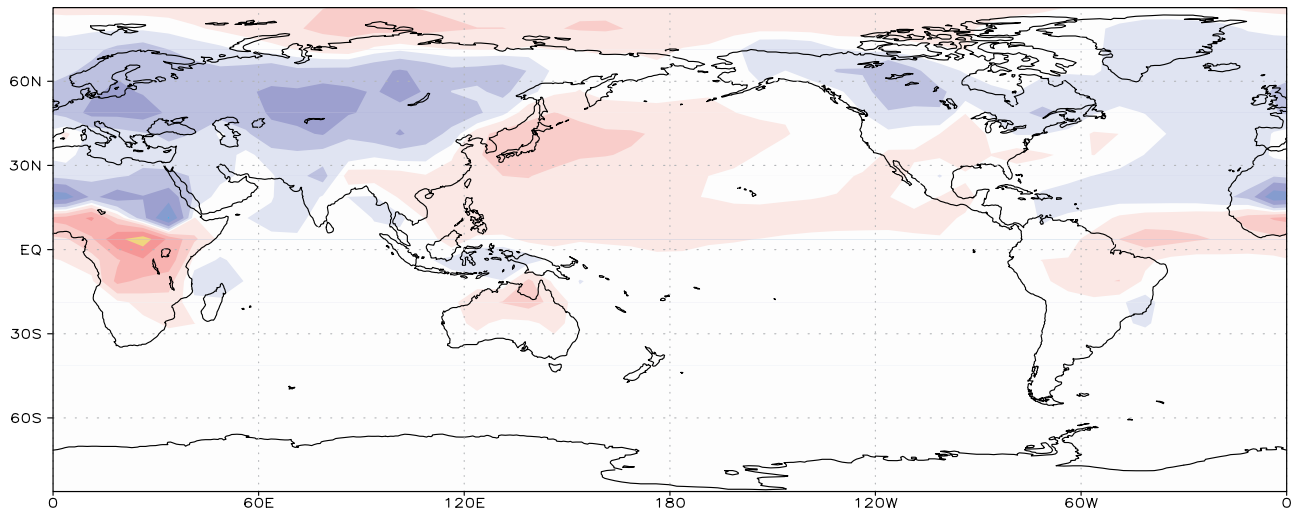
P. Bousquet and P. Ciais, Laboratoire des Sciences du Climat et de l'Environnement, Commissariat à l'Énergie Atomique, L'orme des merisiers, Gif sur Yvette 91191, France. (bousquet@lsce.saclay.cea.fr; ciais@lsce.saclay.cea.fr)

P. Peylin, Laboratoire de Biogéochimie isotopique, CNRS-UPMC-INRA, 4 Place Jussieu, Paris 75005, France. (peylin@lsce.saclay.cea.fr)

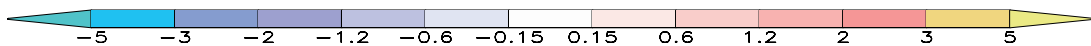
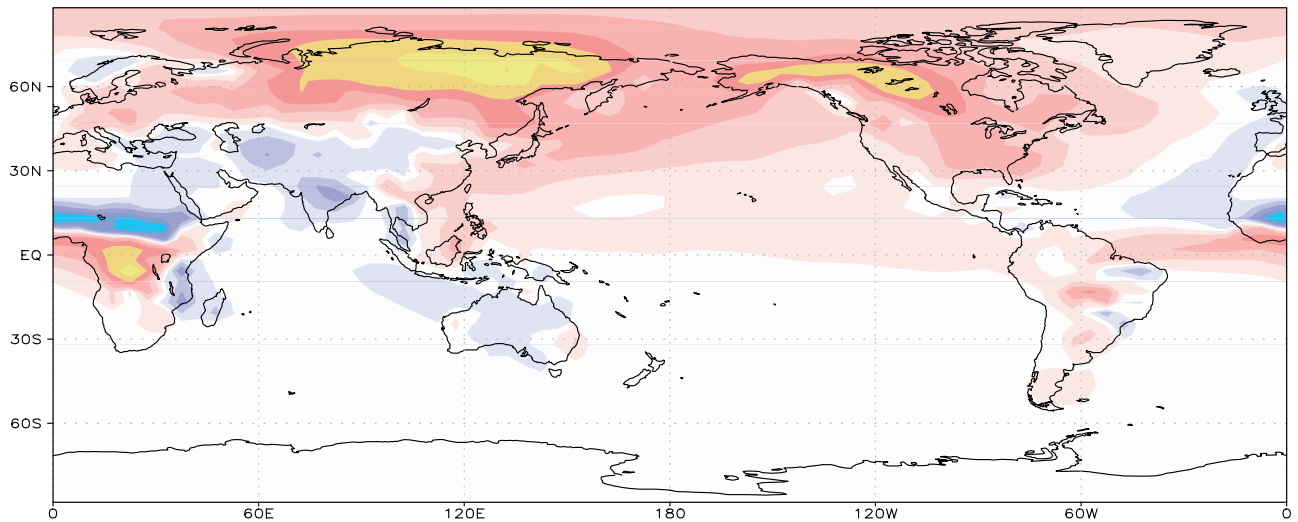
CASA Annual Surface Rectifier, GCTM [ppmv]



SiB2 Annual Surface Rectifier, TM2 [ppmv]



SiB2 Annual Surface Rectifier, TM3 [ppmv]



---

**Figure 9.** (opposite) (a) Annual CO<sub>2</sub> concentration (ppm) simulated by TM2, TM3, and GCTM at all 46 stations with the a priori sources and sinks as defined before the inverse optimization, along with the observed concentrations. Stations are ordered by increasing latitude. (b) Contribution of the fossil fuel emissions only to the annual total concentration in Figure 9a. (c) Contribution of the annually balanced land biosphere only to the annual total concentration in Figure 9a.